Copy 6
RM L54D22

NACA RM L54D22

NACA

RESEARCH MEMORANDUM

WIND-TUNNEL EXPERIMENTS CONCERNING THE DYNAMIC BEHAVIOR OF A LOW-SPEED SLOWLY SPINNING FIN-STABILIZED ROCKET

By John D. Bird and Jacob H. Lichtenstein

Langley Aeronautical Laboratory
Langley Field, Va.

NATIONAL ADVISORY COMMITTEE
FOR AERONAUTICS

WASHINGTON

July 6, 1954

NACA RM L54D22

[redacted]

NATIONAL ADVISORY COMMITTEE FOR AERONAUTICS

RESEARCH MEMORANDUM

WIND-TUNNEL EXPERIMENTS CONCERNING THE DYNAMIC BEHAVIOR OF A LOW-SPEED SLOWLY SPINNING FIN-STABILIZED ROCKET

By John D. Bird and Jacob H. Lichtenstein

SUMMARY

An investigation was made in the Langley stability tunnel to determine the effectiveness with which the dynamic characteristics of a low-speed slowly spinning fin-stabilized rocket could be studied by a free-oscillation technique and to study certain peculiarities of behavior that have been observed for this type of missile. The testing system employed permitted the model freedom to roll, yaw, and precess and enabled the application of initial disturbances similar to those experienced in actual firings.

Satisfactory demonstrations were made of an instability encountered by this missile in cross-wind firings, and of the effectiveness of reversing the direction of rotation of the arming propeller in alleviating, and the effectiveness of adding a spoiler nose ring in completely eliminating, this instability. The theoretical calculations confirmed these results and indicated the instability to be caused by the aerodynamic asymmetry associated with arming-propeller rotation and body spin. As a result of these and other observations it is felt that dynamic tests of a spinning missile on a mounting system of the type employed herein offer an excellent means for studying disturbed motions under controlled conditions for those designs where the translatory degrees of freedom are unimportant.

INTRODUCTION

Recently considerable interest has been shown in the stability of spinning missiles because of the increased use of this type of weapon and the existence of an undesirable short-round phenomenon. This phenomenon consists of the development of a large-amplitude whirling motion which persists throughout the flight of the missile and considerably

[redacted]

shortens the range because of the large drag at the high angles of yaw involved. Such performance, if of frequent occurrence, places a severe limitation on the usefulness of these weapons. Observations have shown that the motion consists of a precession of the missiles about the flight path at an angle of yaw, much in the manner of a top precessing about the vertical. Results from the Langley stability tunnel indicate that the instability of one missile of this type, an antisubmarine rocket, is closely associated with the existence of an unstable Magnus effect which varies nonlinearly with angle of yaw and thus only takes effect when disturbances of sufficiently large magnitude are experienced on firing. It has been shown that this Magnus effect could be diminished by reversal of the direction of rotation of an arming propeller which was mounted on the nose of the model and almost completely destroyed by the addition to the nose of the model of a ring made of small welding rod. Reference 1 shows by calculation that larger disturbances are experienced by this rocket when launched to starboard from a moving ship than when launched to port and that, for a rocket having the Magnus effects indicated in the Langley stability tunnel tests, instability of the type discussed may be obtained. From these results it can be seen that this instability will occur at lower forward speeds of the ship, and thus smaller initial cross winds, for firings made to starboard than for firings made to port. The difference in characteristics of the missile when fired to starboard and to port is shown to arise from the fact that in firings made to starboard from a moving ship the missile is initially urged by muzzle tip-off (the act of falling from the muzzle) in the direction in which the rocket normally precesses under the influence of the stability produced by its tail fins, and the gyroscopic effects involved; whereas in firings made to port the opposite is true. This condition results in the assumption of different angles of yaw and the absorption of different amounts of energy from the Magnus influence during the initial stages of the motion in the two cases. Typical records of satisfactory and unsatisfactory flights of this type of missile are shown in the form of polar plots in figure 1 for illustration of the motion just described. The angle of yaw of the missile axis to the relative wind is plotted as the radius and the angle of precession of the missile axis as the azimuth. The satisfactory flight was to port, and the unsatisfactory to starboard.

The purpose of the present investigation was to determine the effectiveness with which the dynamic characteristics of a spinning missile having the peculiarities of behavior outlined herein could be studied by a free-oscillation technique and to confirm by experiments with such a system and with supplementary calculations the conclusions reached in reference 1. For this purpose, a testing system was devised wherein various disturbances could be applied to a 1/2-scale dynamic model of the antisubmarine rocket previously mentioned. The model was mounted on a support strut in the test section of the Langley stability tunnel with freedom to spin under the action of its canted fins, to change angle of yaw, and to precess. The translatory degrees of freedom are not

included in this scheme; however, their omission was felt not to be of major importance for the problem at hand.

By utilizing this setup, a series of tests were conducted wherein the influence of simulated firings to port and starboard were studied for various arming-propeller arrangements and rates of spin. The different spin rates were obtained by the use of a series of stabilizing-fin arrangements incorporating various helix angles. Some calculations were made on a Reeves Electronic Analog Computer for comparison with the experimental results.

SYMBOLS

The results are presented relative to the Eulerian system of axes shown in figure 2 in which positive directions of moments, angles, and angular velocities are indicated by arrows. The symbols and coefficients are defined as follows:

θ angle of yaw of longitudinal missile axis with respect to flight path, radians

$\dot{\theta} = \frac{\partial \theta}{\partial \tau}$

$\ddot{\theta} = \frac{\partial^2 \theta}{\partial \tau^2}$

ψ angle of precession of longitudinal missile axis about flight path, radians

$\dot{\psi} = \frac{\partial \psi}{\partial \tau}$

$\ddot{\psi} = \frac{\partial^2 \psi}{\partial \tau^2}$

p nondimensional spin rate about longitudinal missile axis, (Spin rate) $\times \frac{l}{2V}$

ω_x nondimensional total spin rate of missile, (Total spin rate) $\times \frac{l}{2V}$

A moment of inertia of missile about axis normal to longitudinal, slug-ft^2

[redacted]

C moment of inertia of missile about longitudinal axis, slug-ft^2

μ relative density factor, $8A/\rho Sl^3$

$C_{m_\theta} = \frac{\partial C_m}{\partial \theta}$

$C_{m_{\dot{\theta}}} = \frac{\partial C_m}{\partial \dot{\theta}}$

$C_{m_{\dot{\psi}}} = \frac{\partial C_m}{\partial \dot{\psi}}$, a function of θ

$C_{n_{\dot{\psi}}} = \frac{\partial C_n}{\partial \dot{\psi}}$, a function of θ

$C_n(\theta,p)$ lateral-moment coefficient which is a function of θ and p

C_m longitudinal-moment coefficient, M/qSl

C_n lateral-moment coefficient, N/qSl

M moment about nodal axis, ft-lb

N moment about normal to nodal axis, ft-lb

τ nondimensional unit of time, $\frac{2tV}{l}$

t time, sec

q dynamic pressure, $\frac{1}{2}\rho V^2$, lb/sq ft

ρ mass density of air, slugs/cu ft

V forward velocity, ft/sec

S maximum cross-sectional area of missile, sq ft

l length of missile, ft

X,Y,Z coordinate axes

[redacted]

Apparatus and Tests

The equipment employed in these tests consisted of a 1/2-size dynamically scaled model of the antisubmarine rocket and a suitable mounting system, a tripper which served to give the proper initial disturbance to the model, a periscope for observation purposes, and cameras for recording the model motions. Figure 3 shows some of this equipment mounted in the test section and diffuser of the Langley stability tunnel.

The model employed for these tests was constructed basically of mahogany. Lead was used for ballast to obtain dynamic similarity between test and free-flight conditions. Figure 4 is a sketch showing details of the model construction. Overall dimensional and inertial characteristics are given in table I. Movable weights were used to compensate for the addition of small components such as arming propellers and nose rings in order to maintain the center of gravity of the model at the normal center-of-gravity location of the rocket. The front and rear portions of the model were mounted on a shaft that was supported by ball bearings in the center portion. This arrangement left the greater portion of the model free to spin in response to the action of the stabilizing fins which were set at an angle with respect to the model center line. The center section of the model, the exposed portion of which was $7\frac{1}{4}$ inches in length, did not spin in order to allow attachment to the supporting strut. Aluminum skirts were employed to cover the joint and so reduce leakage between the center section and the rotating front and rear portions of the model.

A number of different ancillary components were employed in the tests. These included three arming-propeller configurations, three stabilizing-fin arrangements, and a spoiler nose ring. One arming-propeller configuration was that with which the missile was originally designed and which rotated opposite to the direction of rotation of the missile. The second arming propeller was the same size as the original propeller but rotated opposite to the direction of the original propeller. The third arming propeller was geometrically similar but 50 percent larger in diameter than the other two and rotated opposite to the direction of the original propeller. The three stabilizing-fin arrangements, which consisted of fins and shroud, were geometrically similar, but the fins had cants of 3°, 7° (original), and 10°. All three fin arrangements were designed to produce spin of the model in the positive sense (figs. 2 and 4). The spoiler nose ring was made of 1/16-inch welding rod, and was $6\frac{3}{8}$ inches in outside diameter.

The model was mounted on the support strut by a ball-bearing gimbal system at a position corresponding to the normal center-of-gravity location of the rocket. This system permitted the model to change angle of

[redacted]

yaw and to precess in much the same manner as in free flight. The friction in the ball-bearing gimbal was kept as low as possible during the tests, of course. Safety cables 1/8 inch in diameter were stretched across the tunnel in such manner as to form an octagonal region about 30 inches between wires in which the tail of the model was located. These cables restricted the angle of yaw of the model to about 35° and thus prevented the gimbal from being damaged when unstable conditions were encountered.

The tripper was a device which served to hold the missile at an angle of yaw corresponding to a chosen side wind and to give a scale disturbance in precession corresponding to the effect of the tip-off that occurs as the rocket leaves the muzzle of the launcher. The details of construction of this device are shown in figure 5. The tripper was connected through a self-alining ball bearing to a 5/16-inch-diameter trunnion which was attached to the rear of the model in line with its longitudinal axis. This connection permitted the model to spin in response to the airstream and fins prior to release.

The tripper could be located at various positions in the test section in order to simulate various degrees of initial side wind. These various positions may be employed to simulate the disturbance experienced by the rocket in firings to starboard or port from a moving ship. With the tail held to the right or left when facing the wind, a downward flip of the tail corresponds to the disturbance experienced in firings to starboard and port, respectively. The periscope shown in figure 3 was employed to observe the motion of the model which resulted from the initial condition imposed by the tripper. This piece of equipment was mounted downstream of the model location so that a measure of both the angle of yaw and precession could be obtained.

A still camera rigged for time exposures and a motion-picture camera were mounted about 60 feet downstream of the model location for making records of the tests. The still camera was used to record the motion of the tail of the model. This was accomplished by the use of a grain-of-wheat lamp attached at the rear of the model in the trunnion employed for applying disturbances. With all other lights extinguished traces of the motion of the bulb were obtained during time exposures. These traces when obtained from the rear of the model as was done in these tests are polar plots wherein the radius is proportional to the angle of yaw of the model and the azimuth angle is the amount that the model has precessed. The motion-picture camera was used to check the results of the still camera and to obtain illustrative scenes of the model motion with full illumination.

All tests were conducted in the 6- by 6-foot test section of the Langley stability tunnel at a dynamic pressure of 39.7 pounds per square foot which corresponds to a Mach number of 0.17 and a Reynolds number

of 4.84×10^6 based on model length. Tests were made to study the influence of arming-propeller configuration, spoiler nose ring, and rates of spin on the dynamic characteristics of the model for simulated firings to port and starboard at initial yaw angles to 30°. In one case the effect of decreasing the tip-off impulse was determined. Table II is a list of the tests made.

Theoretical Calculations

A series of calculations were made on a Reeves Electronic Analog Computer for comparison with the results of the experiments. These calculations, with the exception of spin, included the same degrees of freedom as were employed in the experiments, namely, angle of yaw and precession. A constant value which was obtained by averaging actual missile firing data was used for the total spin rate. The equations of motion employed were

$$\left(\ddot{\theta} + \omega_x \frac{C}{A} \dot{\psi} \sin \theta - \dot{\psi}^2 \sin \theta \cos \theta\right)\mu - C_{m_\theta}\theta - C_{m_{\dot{\theta}}}\dot{\theta} - C_{m_{\dot{\psi}}}\dot{\psi} = 0$$

$$\left(\ddot{\psi} \sin \theta - \omega_x \frac{C}{A} \dot{\theta} + 2\dot{\theta}\dot{\psi} \cos \theta\right)\mu + C_{n_{\dot{\psi}}}\dot{\psi} + C_n(\theta, p) = 0$$

where

$$\omega_x = p + \dot{\psi} \cos \theta = 0.588$$

and θ and ψ are the Euler angles as defined in figure 2. These equations are effectively those of a top with appropriate aerodynamic terms added. Derivations of like equations may be seen in references 2 and 3.

Calculations of the disturbed motions of the rocket were made for comparison with the experimental results for simulated firings to port and starboard at initial angles of yaw up to about 30°. The appropriate tip-off impulse was obtained from actual firings (ref. 4). The conditions for which these calculations were made are listed in table III. The aerodynamic and inertial constants used are given in table I and figure 6.

RESULTS AND DISCUSSION

Presentation of Results

The results of the investigation are presented in figures 7 to 20. A list of all tests conducted, including an index to the figures giving experimental results and certain comments thereon, is given in table II. A list of the conditions for which theoretical calculations were made for comparison with the experiments is given in table III. A majority of the experimental data were from photographic traces of the bulb attached to the rear of the model. Figures 7, 11, 14, and 18, however, were either wholly or in part traced from motion-picture records.

Stability of Original Model

The experimental dynamic characteristics of the original model for simulated firings (fig. 7) show general agreement with theoretical calculations (fig. 8) and actual firings in that large-amplitude whirling motions developed that were more readily obtained for simulated firings to starboard than to port. In addition, the division between good and bad performance was clearly defined as in the full-scale tests, there being no appreciable borderline region (ref. 5). A small residual motion developed near the end of all stable runs made for the basic missile. This effect is believed to be associated with the asymmetric moment which existed at zero yaw. This was verified by the exclusion of this quantity in certain theoretical calculations. No particular importance is attached to this effect because its amplitude is no more than 5°.

One condition where the results (fig. 7) did not agree with either actual firings or with theoretical calculations (fig. 8) was at zero yaw where the experiment indicates the model to be unstable. An experiment in which the tip-off impulse was reduced by about 10 percent produced a satisfactory response of the model; this result indicates a marked sensitivity to this factor (fig. 11). An examination of the information from which the design tip-off impulse was calculated (ref. 4) indicates the possibility of an error considerably larger than this amount. The theoretical calculations also showed this sensitivity to the magnitude of the tip-off impulse, because an increase in the initial tip-off condition of only 15 percent showed that the response was unstable (fig. 12(a)).

The fact that the experiment and calculations do not agree for the condition of the tail 10° to the right may also be a result of this sensitivity to the magnitude of the tip-off impulse since a decrease of 20 percent in the value used for the calculations produced a satisfactory response. This sensitivity to the magnitude of the tip-off impulse, however, is not uniform throughout the yaw range but is largest where

[redacted]

the behavior of the missile changes from stable to unstable. For 15° tail to the right, for instance, a decrease in the tip-off impulse to one-half of the value normally used for the calculations failed to produce a stable response.

Effect of Reversing Direction of Arming Propeller

Reversing the direction of rotation of the arming propeller effected a considerable improvement in the dynamic behavior of the model (fig. 9). Instability was eliminated for simulated firings to port and at zero yaw and was restricted to angles greater than 15° for simulated firings to starboard. The residual motion existing for the original model was not detected. The calculated results are in good agreement with experiment and also show the beneficial effects of reversing the arming-propeller rotation (fig. 10). For this case it was necessary to increase the tip-off impulse used in the calculations at 2° yaw by 90 percent before an unstable condition developed (fig. 12(b)).

Effect of Increasing Size of Reversed-Rotation Arming Propeller

Increasing the diameter of the reversed-rotation arming propeller by 50 percent eliminated the instability of the original model for firings to starboard but introduced poorer performance than that of the model with the small reversed rotation propeller for firings to port and at zero initial yaw (fig. 13). For these conditions the damping of the motion was poor. This effect is felt to be attributable to a reverse aerodynamic asymmetry similar to that indicated for the basic model at zero angle of yaw in figure 6(c), but of larger magnitude.

Effect of Removing Arming Propeller

Removing the arming propeller produces an effect on the dynamic behavior of the model similar to reversing the direction of rotation of the arming propeller (fig. 14). Instability was obtained for a simulated firing to starboard at 20° initial yaw but not at the other test conditions, including a simulated firing to port at 20° initial yaw.

Effect of Adding Spoiler Nose Ring to Basic Model

Adding the spoiler nose ring to the nose of the original model eliminated all unstable performance of the model (fig. 15). The calculated results for this condition are in good agreement with experiment (fig. 16). Calculations using data from a previous test in the Langley stability tunnel indicate only a 1-percent loss in range as a result of the addition of this device to the missile.

[redacted]

Effect of Changes in Spin Rate

Reducing the spin rate of the model by installing the 3° tail made no appreciable improvement in stability except when the tail was held initially 20° to the left (fig. 17(a)). In this case, however, the spin rate at release for some reason, probably as a result of mechanical friction, was exceedingly low (table II), such that the expected asymmetrical aerodynamic and inertial moments were not realized. As was the case for the original model configuration, installation of the spoiler nose ring eliminated the instability (fig. 17(b)). The initial spin rate with the 3° tail and the spoiler nose ring was considerably higher than without the nose ring (table II), and a slower rate of damping with the spoiler installed resulted. Increasing the rate of spin of the model by installing the 10° tail eliminated the instability that existed for the original model at zero initial yaw (fig. 18) but, other than for increasing the precessional rate, had little effect on the results for the other initial conditions shown.

The model with no spin equipped with the normal propeller exhibited a mild instability when the tail was held initially 20° to the right (starboard, fig. 19(a)). This instability was caused by the aerodynamic asymmetry arising from the rotation of the arming propeller and does not exist when the propeller is removed (fig. 19(c)). Calculations of the motion of the model show this same effect (fig. 20). Installing a spoiler nose ring on the model equipped with the original propeller eliminates this instability (fig. 19(b)).

An instability which is similar in nature to that exhibited by the nonspinning missile with arming propeller could very well exist for nonspinning pointed-nose missiles that have little aerodynamic surface and therefore low damping. This effect is felt to be possible because the data presented in references 6, 7, and 8 for a pointed body indicate that at high angles of attack a yawing moment sufficient to drive such a motion exists at zero sideslip as a result of the development of an asymmetrical trailing-vortex system.

SUMMARY OF RESULTS

From an investigation in the Langley stability tunnel of the dynamic characteristics of a free-spinning model of an antisubmarine rocket which was mounted with freedom to spin, yaw, and precess the following observations can be made:

1. The tests satisfactorily demonstrated the instability encountered by this antisubmarine rocket in cross-wind firings and showed the effectiveness of reversing the direction of rotation of the arming propeller

in alleviating, and the effectiveness of adding a spoiler nose ring in completely eliminating, this instability. Theoretical calculations confirmed these results and indicated the instability to be caused by the aerodynamic asymmetry associated with arming-propeller rotation and body spin as shown in other papers.

2. In the course of these tests an instability similar to that encountered by the spinning missile was obtained for a nonspinning case. This instability was caused by the aerodynamic asymmetry introduced by the rotation of the arming propeller and could be eliminated without removing the arming propeller by addition of a spoiler nose ring. The asymmetric moment which caused this instability was comparable to that experienced by sharp-nosed bodies at high angles of attack; thus it is possible that pointed nonspinning missiles could have a similar unstable behavior.

3. As a result of this investigation, it is felt that dynamic tests of a spinning missile on a mounting system which provides freedom to spin, yaw, and precess offer an excellent means for studying disturbed motions under controlled conditions for those designs where the translatory degrees of freedom are unimportant.

Langley Aeronautical Laboratory,
National Advisory Committee for Aeronautics,
Langley Field, Va., April 16, 1954.

[redacted]

REFERENCES

1. Miller, A., and Fredette, R. O.: The Motion of a Low Speed, Slowly Spinning Fin Stabilized Rocket, Fired in the Presence of a Crosswind. NAVORD Rep. 3149, Bur. Ordnance, Sept. 22, 1952.

2. Timoshenko, S., and Young, D. H.: Advanced Dynamics. First ed., McGraw-Hill Book Co., Inc., 1948, p. 345.

3. Maple, C. G., and Synge, J. L.: General Equations of Motion for a Projectile With Rotational Symmetry. File No. X 120, Ballistic Res. Labs., Aberdeen Proving Ground.

4. Jones, A. L.: Ballistic Data for the 12.75 Rocket Mk 1 Mod 0. Eleventh Partial Rep. NPG Rep. No. 800, U. S. Naval Proving Ground, Dahlgren, Va., June 18, 1951.

5. Jones, A. L.: Ballistic Calibration of Rockets and Preparation of Rocket Range Tables, Thirteenth Partial Rep. Additional Firing Tests at Sea of the 12.75 Rocket Mk 1 Mod 0, Second Partial Rep. NPG Rep. No. 875, U. S. Naval Proving Ground, Dahlgren, Va., Oct. 1, 1951.

6. Letko, William: A Low-Speed Experimental Study of the Directional Characteristics of a Sharp-Nosed Fuselage Through a Large Angle-of-Attack Range at Zero Angle of Sideslip. NACA TN 2911, 1953.

7. Allen, H. Julian, and Perkins, Edward W.: Characteristics of Flow Over Inclined Bodies of Revolution. NACA RM A50L07, 1951.

8. Kelly, Howard R.: The Subsonic Aerodynamic Characteristics of Several Spin-Stabilized Rocket Models. II. Magnus Coefficients. TN-376, U. S. Naval Ord. Test Station (Inyokern, Calif.), Nov. 12, 1953.

[redacted]

TABLE I

DIMENSIONAL AND INERTIAL CHARACTERISTICS

Characteristics	Full-scale values used in computations	Model values used in tests
Weight, lb	517	-----
Moment of inertia about longitudinal axis, slug-ft^2	2.15	0.068
Moment of inertia about lateral axis, slug-ft^2	57.4	1.85
Length, ft	8.3	4.3
Maximum diameter, ft	1.06	0.53
Cross-sectional area, sq ft	0.886	0.222
Distance from flat of nose to center of gravity, ft	2.32	1.154
Approximate mean rate of spin, rpm	360	Table II
Approximate mean rate of precession, rpm	30	Table II
Forward velocity, fps	275	183.5
C_{m_θ}, per radian	-1.00	-1.00
$C_{m_{\dot{\theta}}}$	-1.9	-1.9
$C_{m_{\dot{\psi}}}$	Figure 6	-----
C_{n_ψ}	Figure 6	-----
$C_n(\theta,p)$	Figure 6	-----

TABLE II

TEST CONDITIONS AND RESULTS

Test	Data on figure	Nose configuration	Propeller configuration	Cant of fins, deg	Initial yaw, deg	Condition simulated	Tip-off	Rotational speed, rpm		Behavior
								Release	Steady	
1	-----	Original	Normal	7 (normal)	0	No side wind	None	-----	1,050	Motion developed slowly to a negative precession at about 30 yaw
2	-----	------do------	------do------	------do------	0	------do------	2/3 normal	750	-----	Motion damped to condition of test 1
3	11	------do------	------do------	------do------	0	------do------	9/10 normal	-----	-----	Do.
4	7	------do------	------do------	------do------	0	------do------	Normal	-----	-----	Unstable; motion developed to a positive precession of about 1.2 cycles per second at 35° yaw where safety wires were encountered
5	7	------do------	------do------	------do------	10 tail to left	Launch to port	------do----	820	-----	Motion damped to condition of test 1
6	7	------do------	------do------	------do------	20 tail to left	------do------	------do----	500	-----	Unstable - same as test 4
7	7	------do------	------do------	------do------	30 tail to left	------do------	------do----	-----	-----	Do.
8	-----	------do------	------do------	------do------	2½ tail to right	Launch to starboard	------do----	780	-----	Do.
9	-----	------do------	------do------	------do------	5 tail to right	------do------	------do----	900	-----	Motion damped to condition of test 1
10	7	------do------	------do------	------do------	10 tail to right	------do------	------do----	1,270	-----	Do.
11	7	------do------	------do------	------do------	15 tail to right	------do------	------do----	1,030	-----	Unstable - same as test 4
12	-----	------do------	------do------	------do------	20 tail to right	------do------	------do----	640	-----	Do.
13	-----	------do------	------do------	------do------	30 tail to right	------do------	------do----	385	-----	Do.
14	9	------do------	Reversed rotation	------do------	0	No side wind	------do----	600	650	Motion damped
15	9	------do------	------do------	------do------	20 tail to left	Launch to port	------do----	550	-----	Do.
16	9	------do------	------do------	------do------	30 tail to left	------do------	------do----	387	-----	Do.
17	-----	------do------	------do------	------do------	10 tail to right	Launch to starboard	------do----	-----	-----	Do.
18	9	------do------	------do------	------do------	15 tail to right	------do------	------do----	850	650	Do.
19	9	------do------	------do------	------do------	20 tail to right	------do------	------do----	-----	-----	Unstable; motion developed to a positive precession of about 1.1 cycles per second at about 30° yaw
20	9	------do------	------do------	------do------	30 tail to right	------do------	------do----	-----	-----	Unstable - same as run 19
21	15	------do------	Large propeller with reversed rotation	------do------	0	No side wind	------do----	650	700	Motion damped slowly
22	15	------do------	------do------	------do------	10 tail to left	Launch to port	------do----	1,040	-----	Motion damped
23	15	------do------	------do------	------do------	20 tail to left	------do------	------do----	600	-----	Motion damped slowly
24	15	------do------	------do------	------do------	30 tail to left	------do------	------do----	405	-----	Do.
25	15	------do------	------do------	------do------	10 tail to right	Launch to starboard	------do----	710	-----	Motion damped
26	15	------do------	------do------	------do------	20 tail to right	------do------	------do----	820	-----	Do.
27	-----	------do------	------do------	------do------	30 tail to right	------do------	------do----	270	700	Do.
28	15	Nose ring added	Normal	------do------	0	No side wind	------do----	680	-----	Do.
29	-----	------do------	------do------	------do------	10 tail to left	Launch to port	------do----	950	-----	Do.
30	15	------do------	------do------	------do------	20 tail to left	------do------	------do----	620	-----	Do.
31	15	------do------	------do------	------do------	30 tail to left	------do------	------do----	450	-----	Do.
32	15	------do------	------do------	------do------	10 tail to right	Launch to starboard	------do----	830	760	Do.
33	15	------do------	------do------	------do------	20 tail to right	------do------	------do----	780	-----	Do.
34	15	------do------	------do------	------do------	30 tail to right	------do------	------do----	420	-----	Do.
35	14	Original	Propeller off	------do------	0	No side wind	------do----	780	770	Do.
36	14	------do------	------do------	------do------	20 tail to left	Launch to port	------do----	580	-----	Do.
37	14	------do------	------do------	------do------	10 tail to right	Launch to starboard	------do----	1,020	-----	Do.
38	14	------do------	------do------	------do------	20 tail to right	------do------	------do----	710	550	Unstable - same as run 19
39	-----	Nose ring added	------do------	------do------	0	No side wind	------do----	670	-----	Motion damped
40	-----	------do------	------do------	------do------	20 tail to right	Launch to starboard	------do----	650	-----	Unstable - same as run 19
41	18	Original	Normal propeller	10	0	No side wind	------do----	1,360	-----	Motion damped
42	-----	------do------	------do------	------do------	20 tail to left	Launch to port	------do----	940	-----	Unstable - precessed at 1.6 cycles per second and about 30° yaw
43	18	------do------	------do------	------do------	10 tail to right	Launch to starboard	------do----	-----	-----	Motion damped
44	18	------do------	------do------	------do------	15 tail to right	------do------	------do----	-----	-----	Unstable - same as run 42 - precessed more rapidly
45	18	------do------	------do------	------do------	20 tail to right	------do------	------do----	1,150	-----	Do.
46	17(a)	------do------	------do------	3	0	No side wind	------do----	308	585	Unstable - precessed at large amplitude
47	17(a)	------do------	------do------	------do------	20 tail to left	Launch to port	------do----	95	385	Motion damped
48	17(a)	------do------	------do------	------do------	20 tail to right	Launch to starboard	------do----	290	-----	Unstable - same as run 46
49	17(b)	Nose ring added	------do------	------do------	0	No side wind	------do----	289	506	Motion damped
50	17(b)	------do------	------do------	------do------	20 tail to left	Launch to port	------do----	250	-----	Do.
51	17(b)	------do------	------do------	------do------	20 tail to right	Launch to starboard	------do----	380	-----	Do.
52	19(a)	Original	------do------	------do------	0	No side wind	------do----	0	0	Do.
53	19(a)	------do------	------do------	------do------	20 tail to left	Launch to port	------do----	-do-	-do-	Do.
54	19(a)	------do------	------do------	------do------	20 tail to right	Launch to starboard	------do----	-do-	-do-	Precessed at fair amplitude in ellipses
55	19(b)	Nose ring added	------do------	------do------	------do------	------do------	------do----	-do-	-do-	Motion damped
56	-----	Original	Propeller Off	------do------	0	No side wind	------do----	-do-	-do-	Do.
57	-----	------do------	------do------	------do------	20 tail to left	Launch to port	------do----	-do-	-do-	Do.
58	19(c)	------do------	------do------	------do------	20 tail to right	Launch to starboard	------do----	-do-	-do-	Do.

TABLE III

CONDITIONS FOR WHICH THE MISSILE MOTIONS WERE COMPUTED

AND THE COMPARABLE TEST CONDITION

Computed condition	Data on figure	Test condition	Data on figure
Normal propeller and 7° tail	8 and 12(a)	Normal propeller and 7° tail	7 and 11
Small reversed propeller and 7° tail	10 and 12(b)	Small reversed propeller and 7° tail	9
Normal propeller, nose ring, and 7° tail	16	Normal propeller, nose ring, and 7° tail	15
Normal propeller and 7° tail, but no spin	20(a)	Normal propeller and 3° tail, but no spin	19(a)
Normal propeller, nose ring, and 7° tail, but no spin	20(b)	Normal propeller, nose ring, and 3° tail, but no spin	19(b)
No propeller, 7° tail, but no spin	20(c)	No propeller, 3° tail, but no spin	19(c)

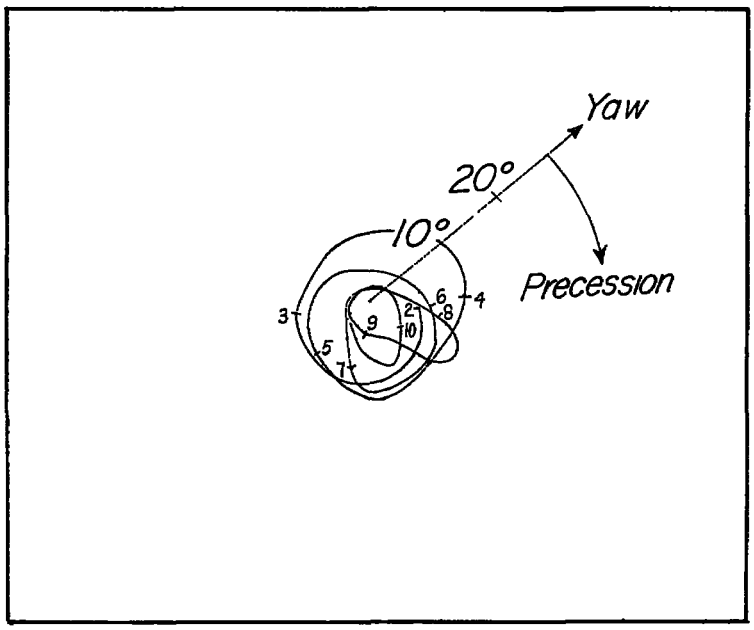

Missile fired to port with a crosswind of 40 knots.

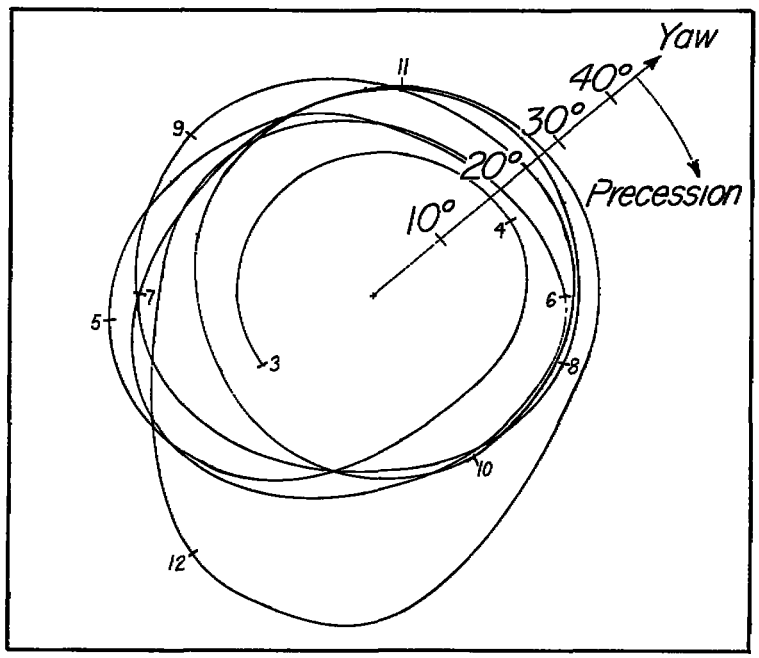

Missile fired to starboard with a crosswind of 34 knots.

Figure 1.- Typical motion of the missile for firings made to port and starboard. Numbered ticks represent elapsed time from firing in seconds.

[redacted]

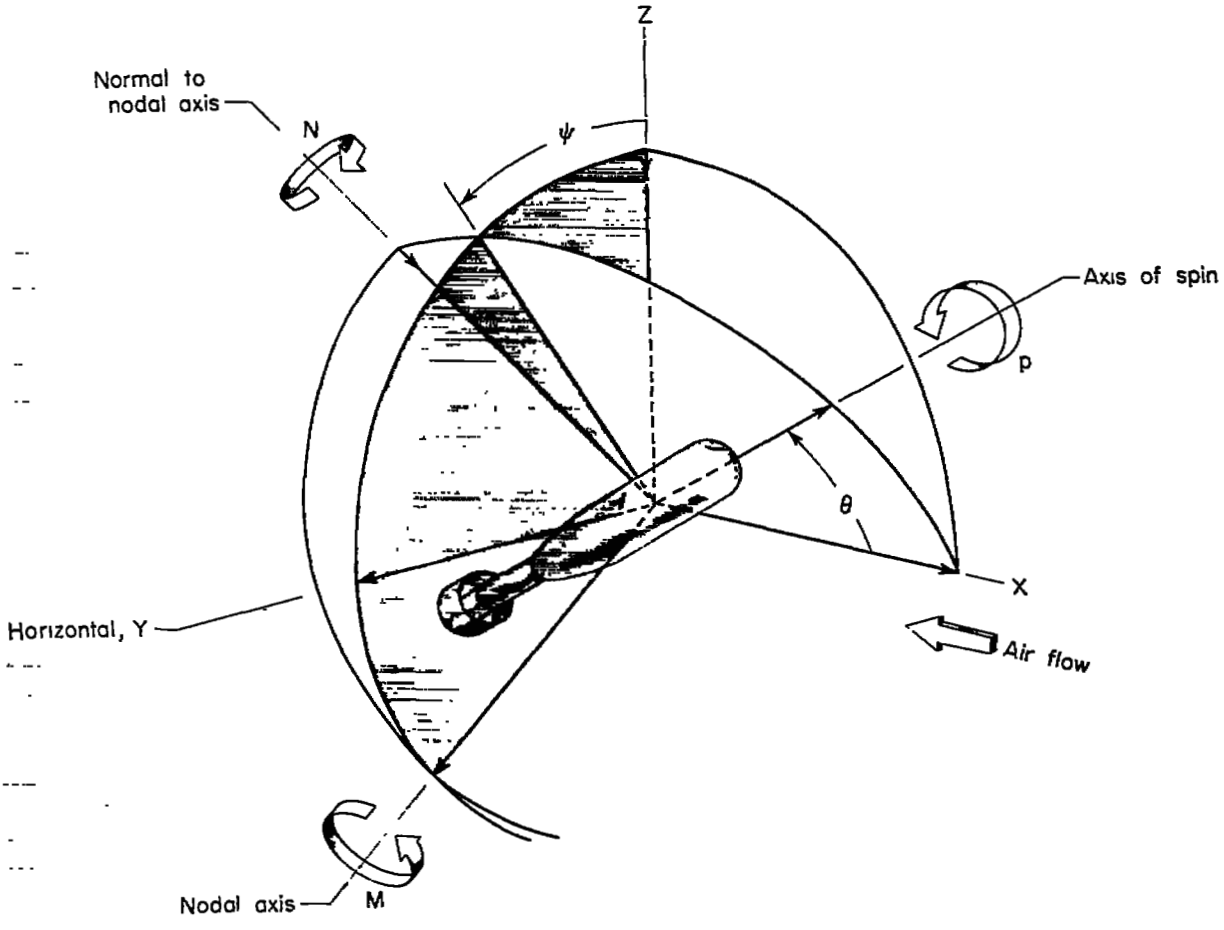

L-83646.1

Figure 2.- System of axes used. Arrows indicate positive direction of forces, moments, angles, and angular velocities.

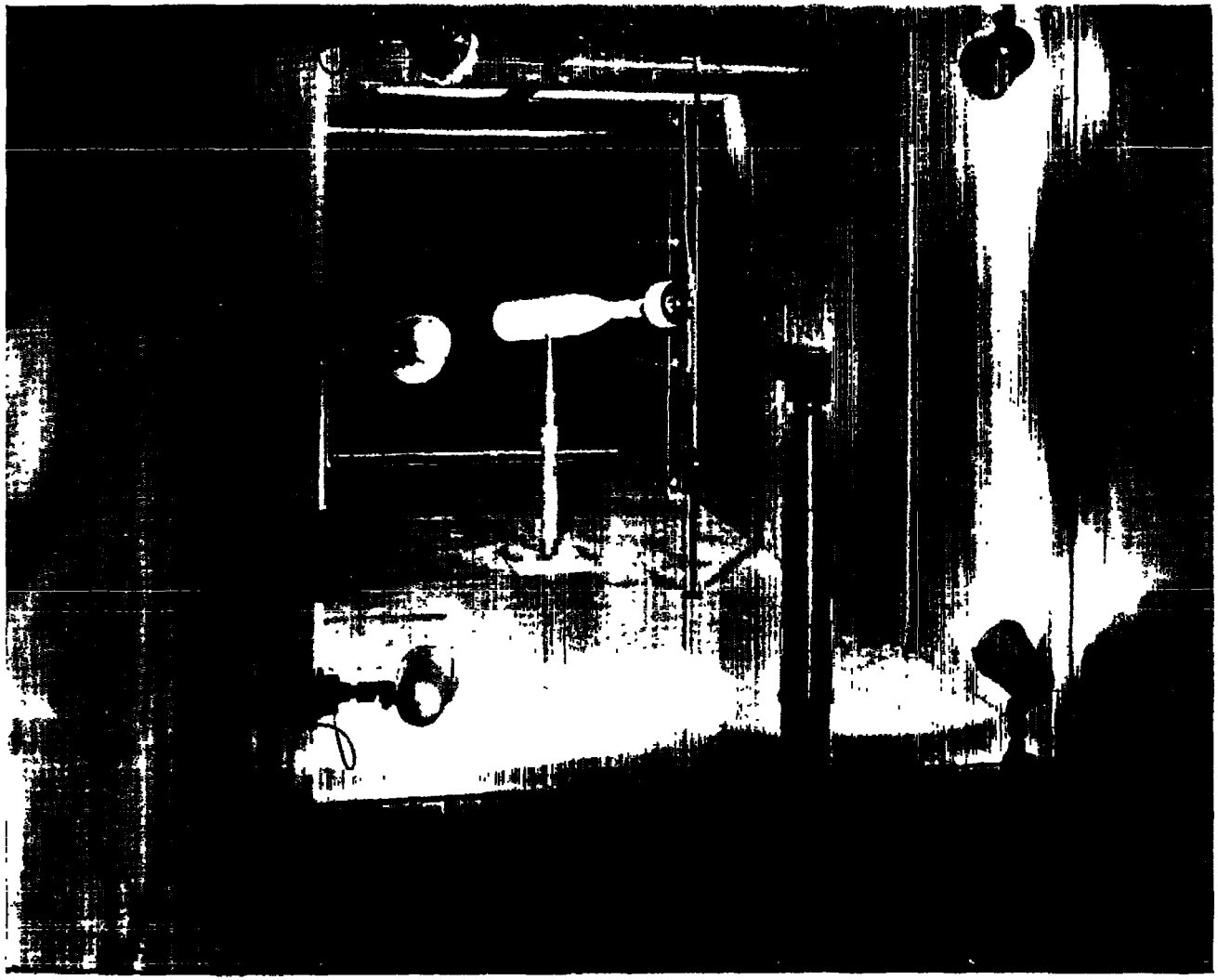

L-80874

Figure 3.- Photograph of the test setup in the Langley stability tunnel showing the model and tripper arrangement and the periscope.

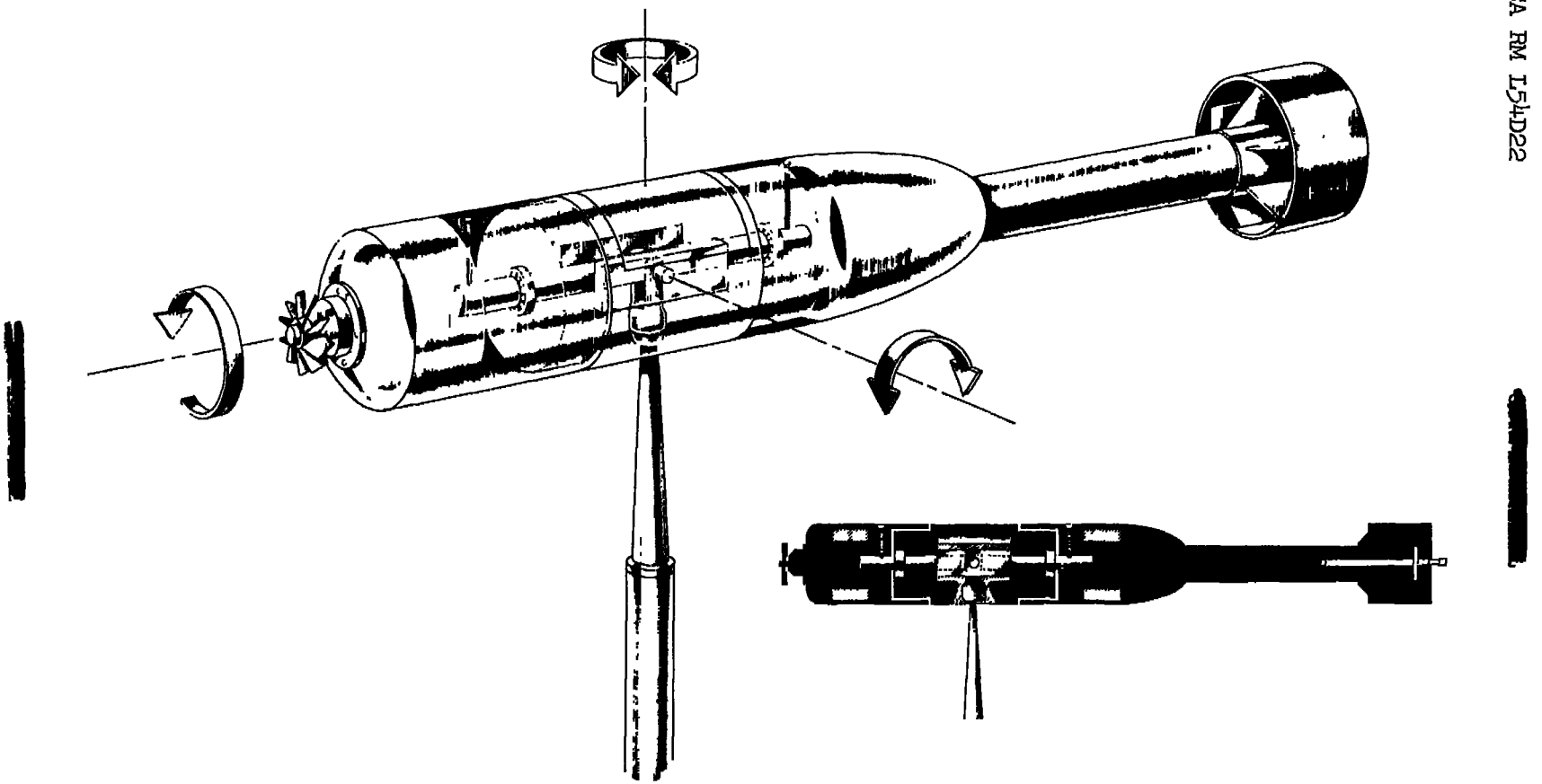

L-83647

Figure 4.- Sketch of the three-degree-of-freedom model and support system.

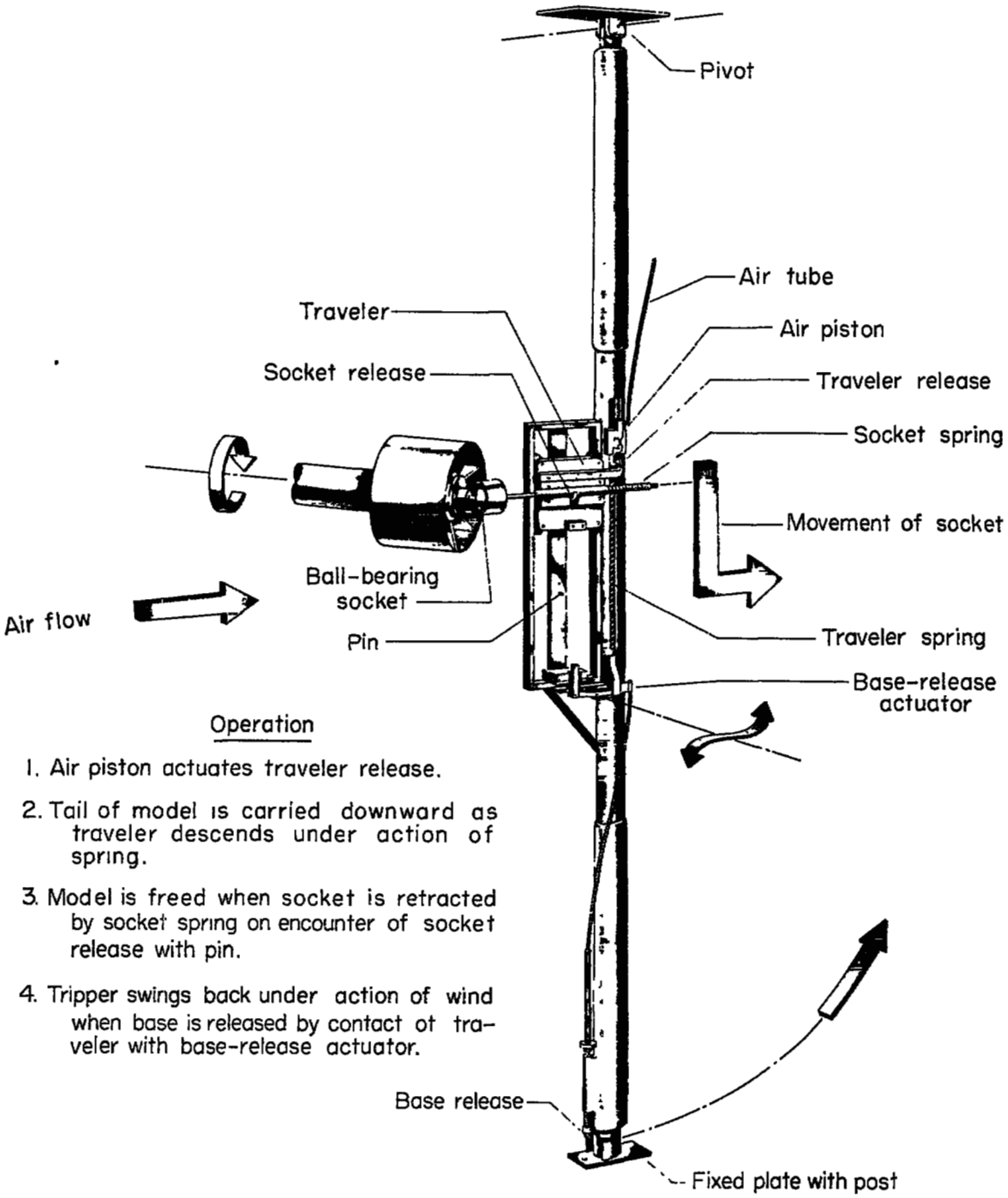

Figure 5.- Sketch of the tripper mechanism as used in the tests.

[redacted]

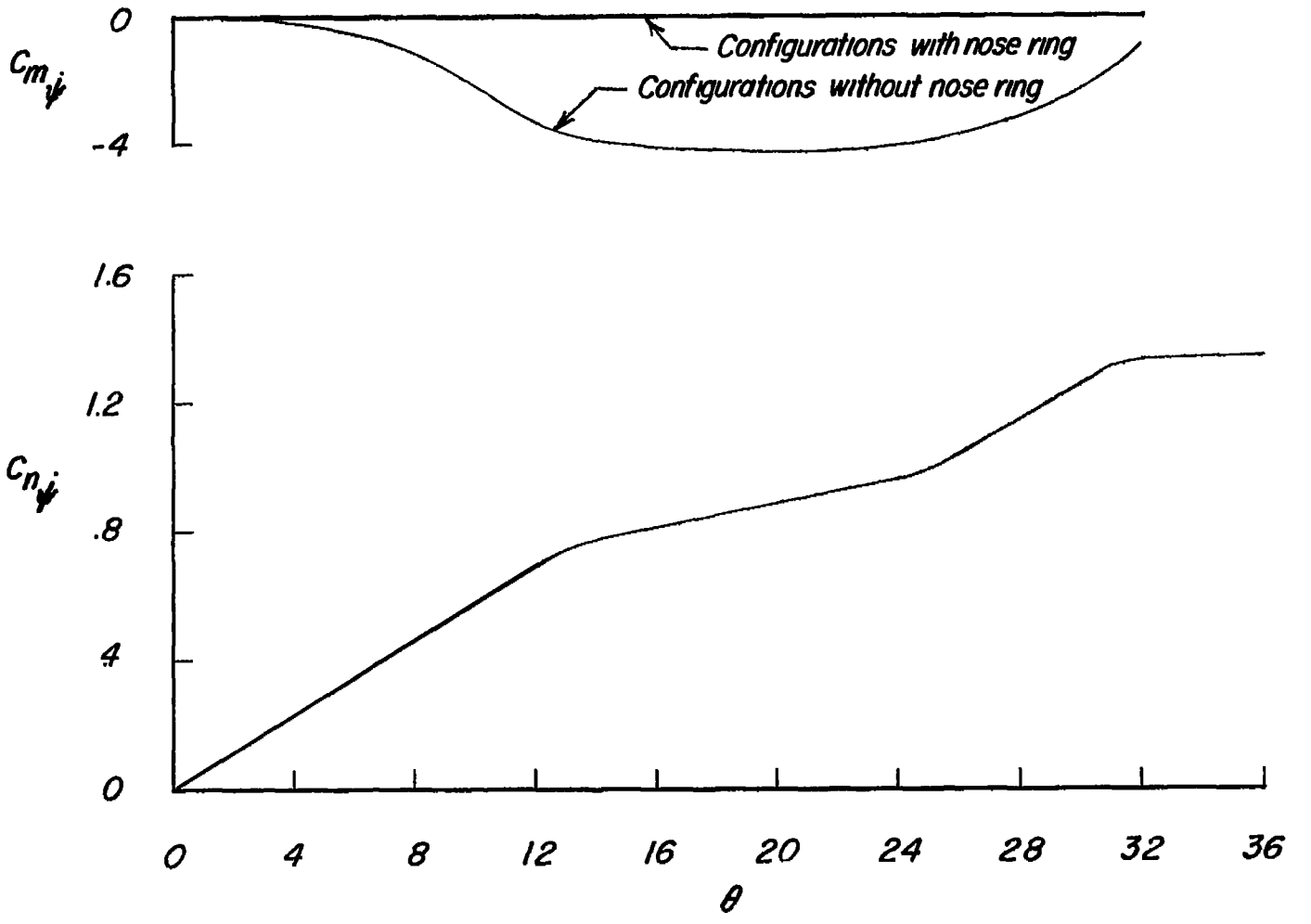

(a) Stationary or spinning model.

Figure 6.- Aerodynamic data for Langley stability tunnel tests used in calculations.

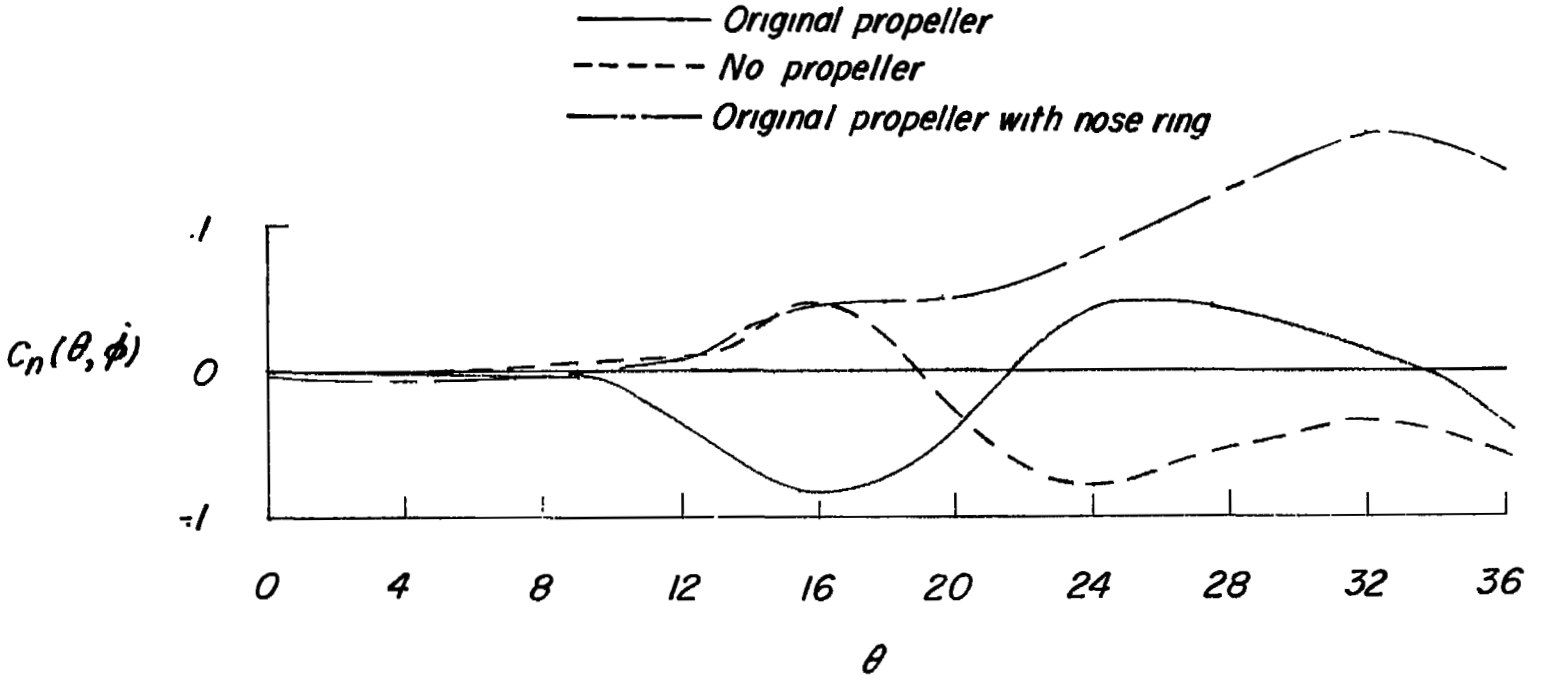

(b) Stationary model.

Figure 6.- Continued.

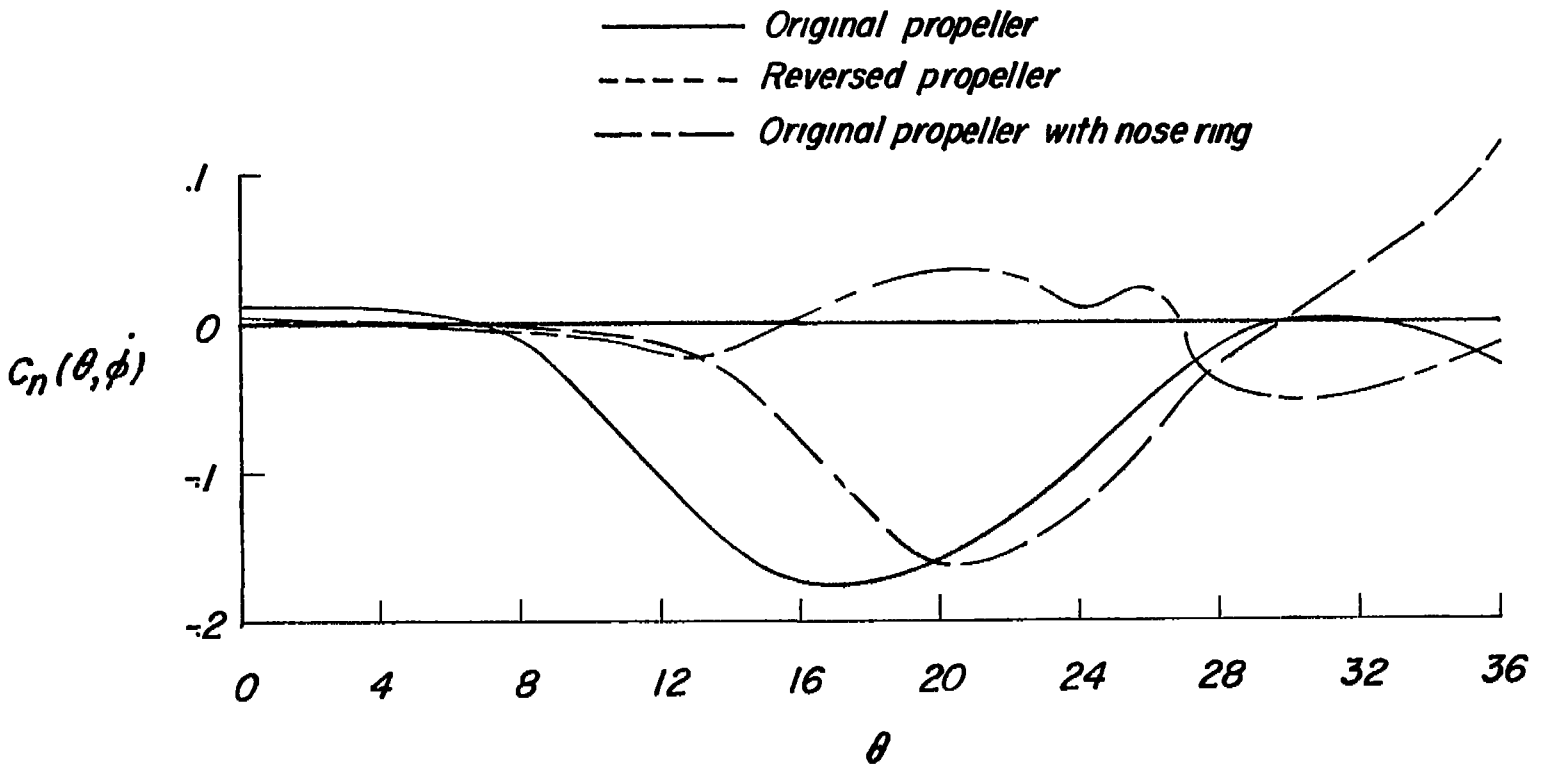

(c) Spinning model.

Figure 6.- Concluded.

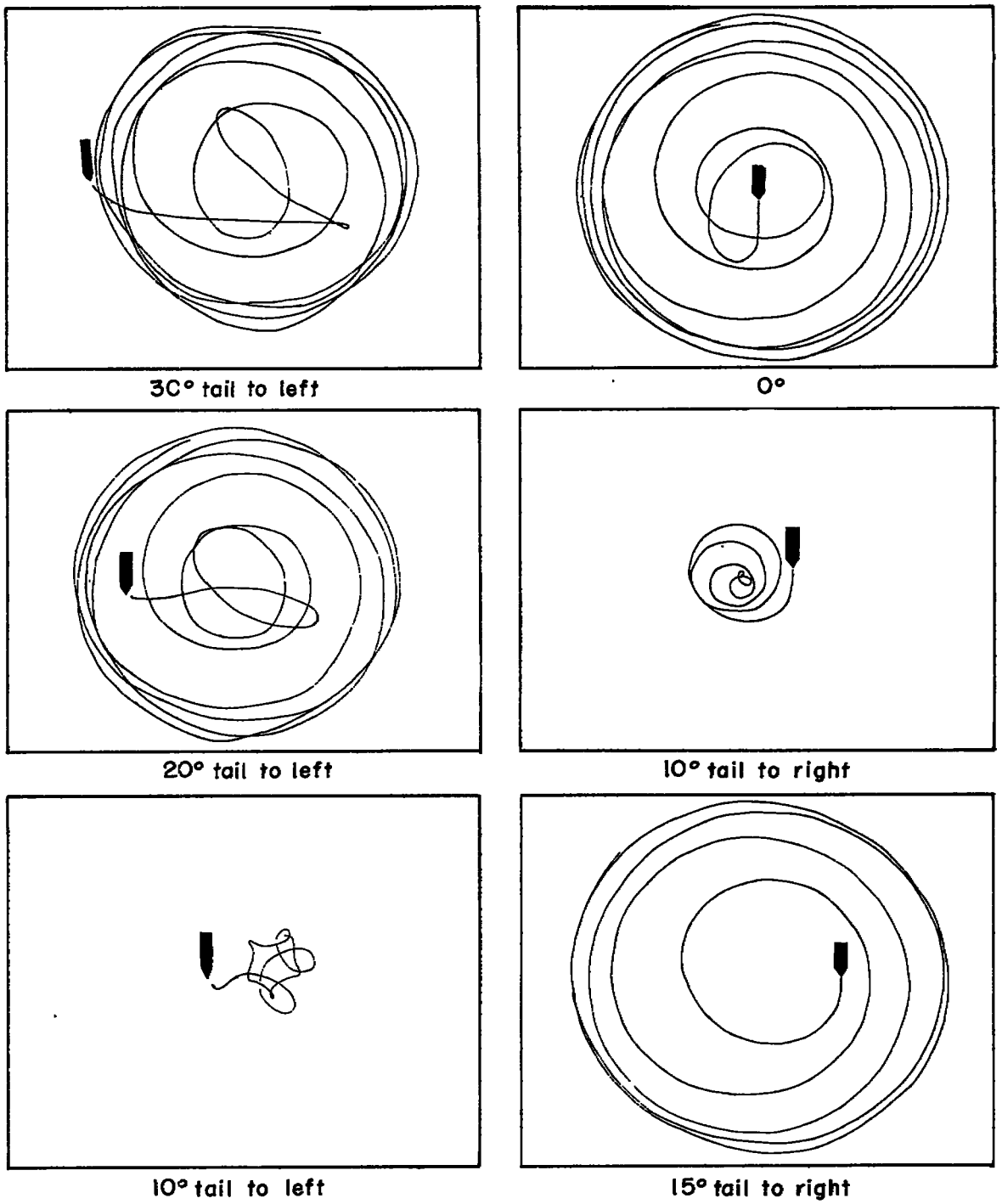

Figure 7.- Experimental motion of model equipped with normal arming propeller and 7° tail for various initial angles of yaw. Tail to left and right simulates firings to port and starboard, respectively. Arrow indicates start of motion and direction of impulse.

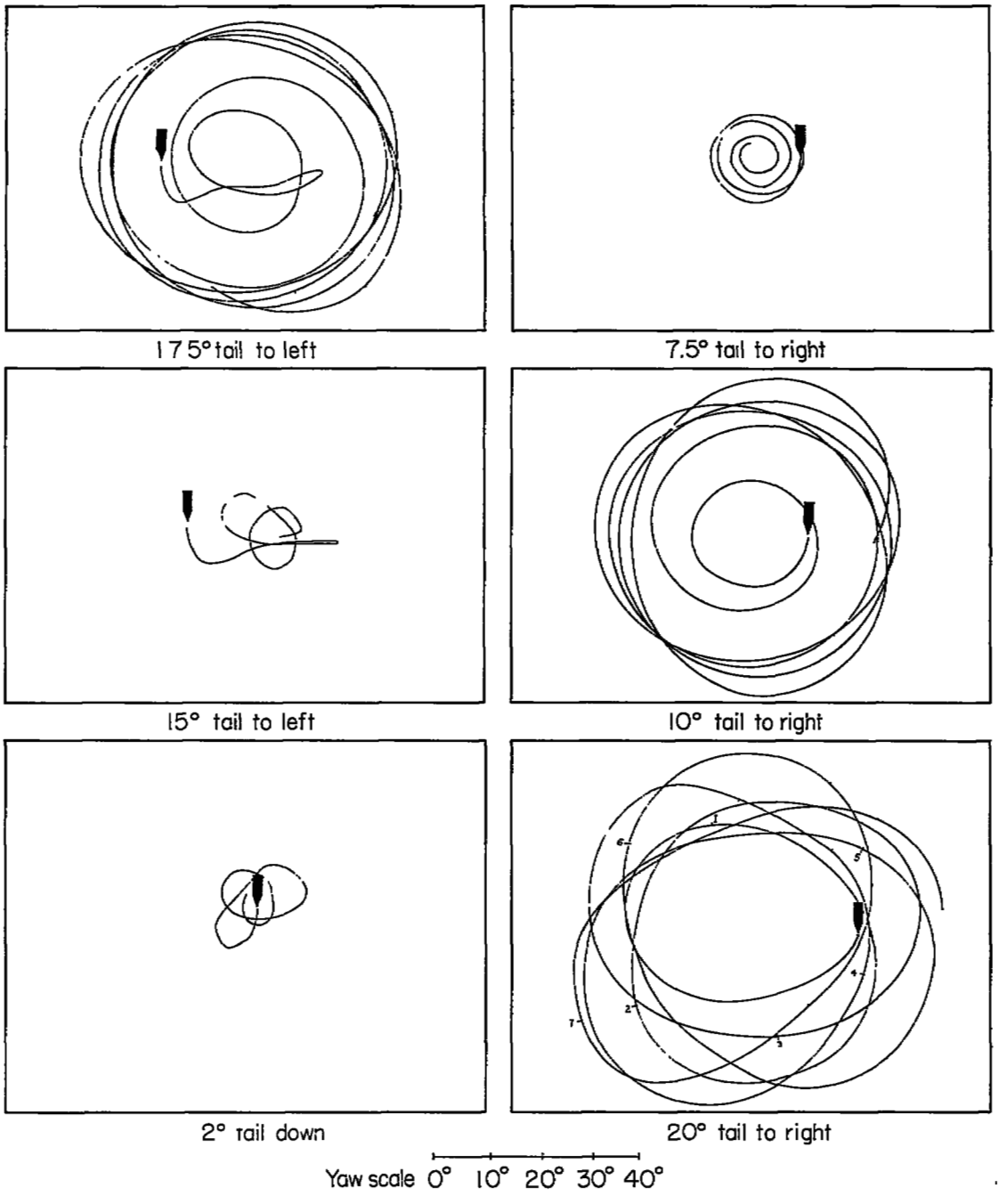

Figure 8.- Calculated motion of model equipped with normal arming propeller and 7° tail for various initial angles of yaw. Tail to left and right simulates firings to port and starboard, respectively. Tick marks represent elapsed time from release in seconds. Arrow indicates start of motion and direction of impulse.

[redacted]

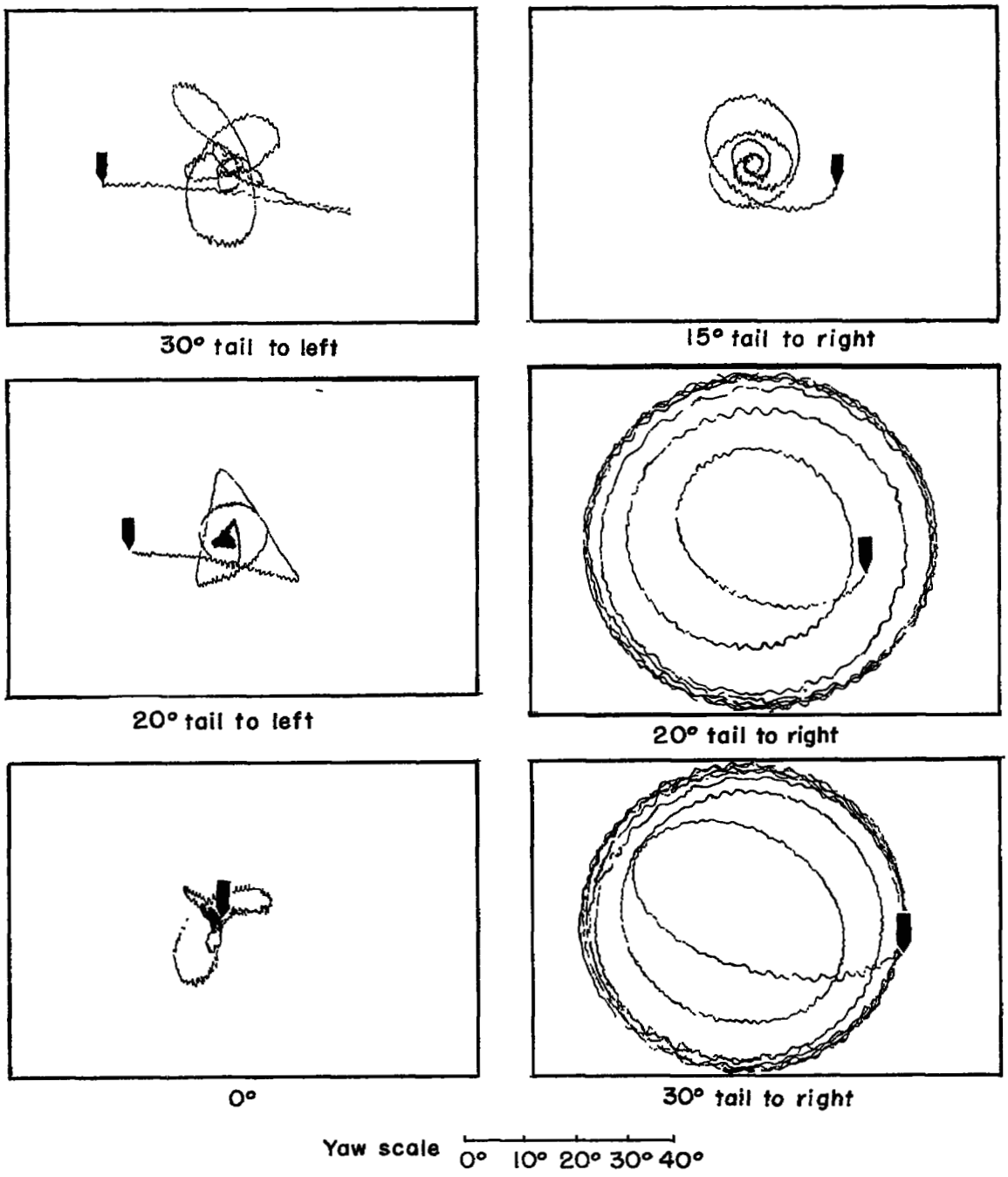

Figure 9.- Experimental motion of model equipped with small reversed-rotation arming propeller and 7° tail for various initial angles of yaw. Tail to left and right simulates firings to port and starboard, respectively. Arrow indicates start of motion and direction of impulse.

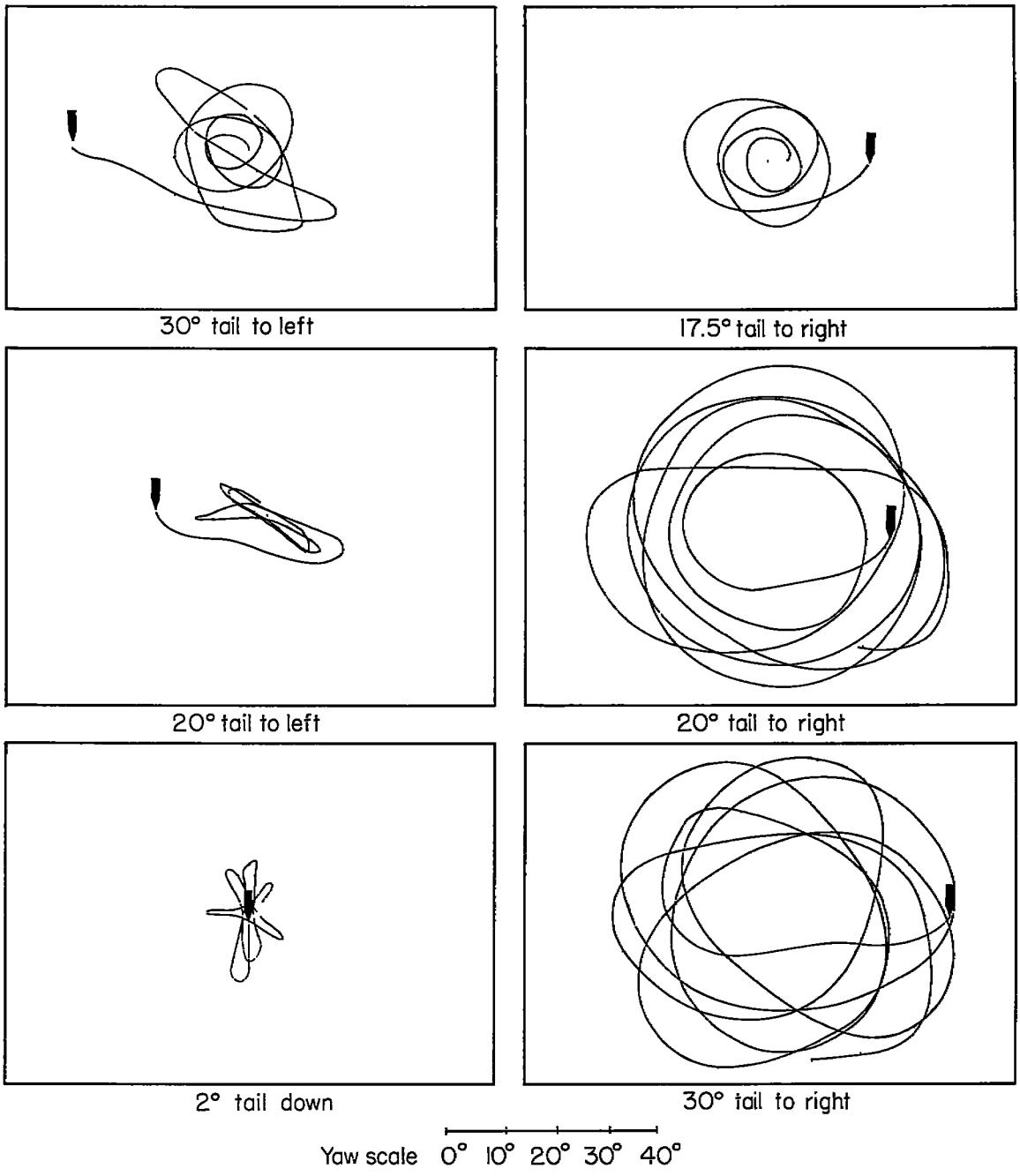

Figure 10.- Calculated motion of model equipped with small reversed-rotation arming propeller and 7° tail for various initial angles of yaw. Tail to left and right simulates firings to port and starboard, respectively. Arrow indicates start of motion and direction of impulse.

[redacted]

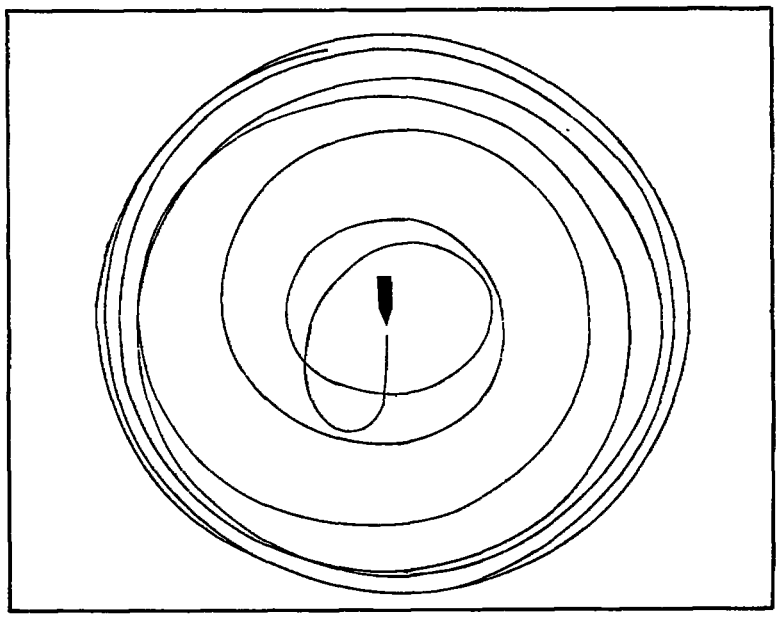

(a) Normal tip-off impulse.

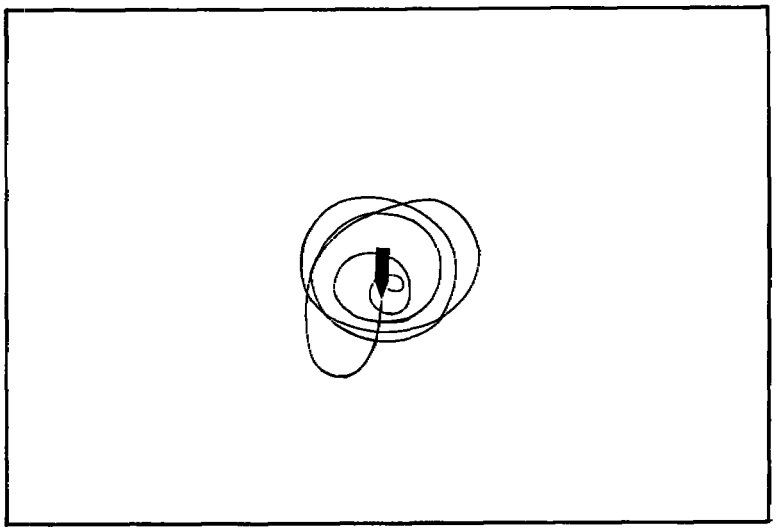

(b) Reduced tip-off impulse.

Yaw scale 0° 10° 20° 30° 40°

Figure 11.- Effect of slightly reducing the tip-off impulse on the experimental motion of the model equipped with the normal arming propeller and 7° tail for zero initial yaw. Arrow indicates start of motion and direction of tip-off impulse.

[redacted]

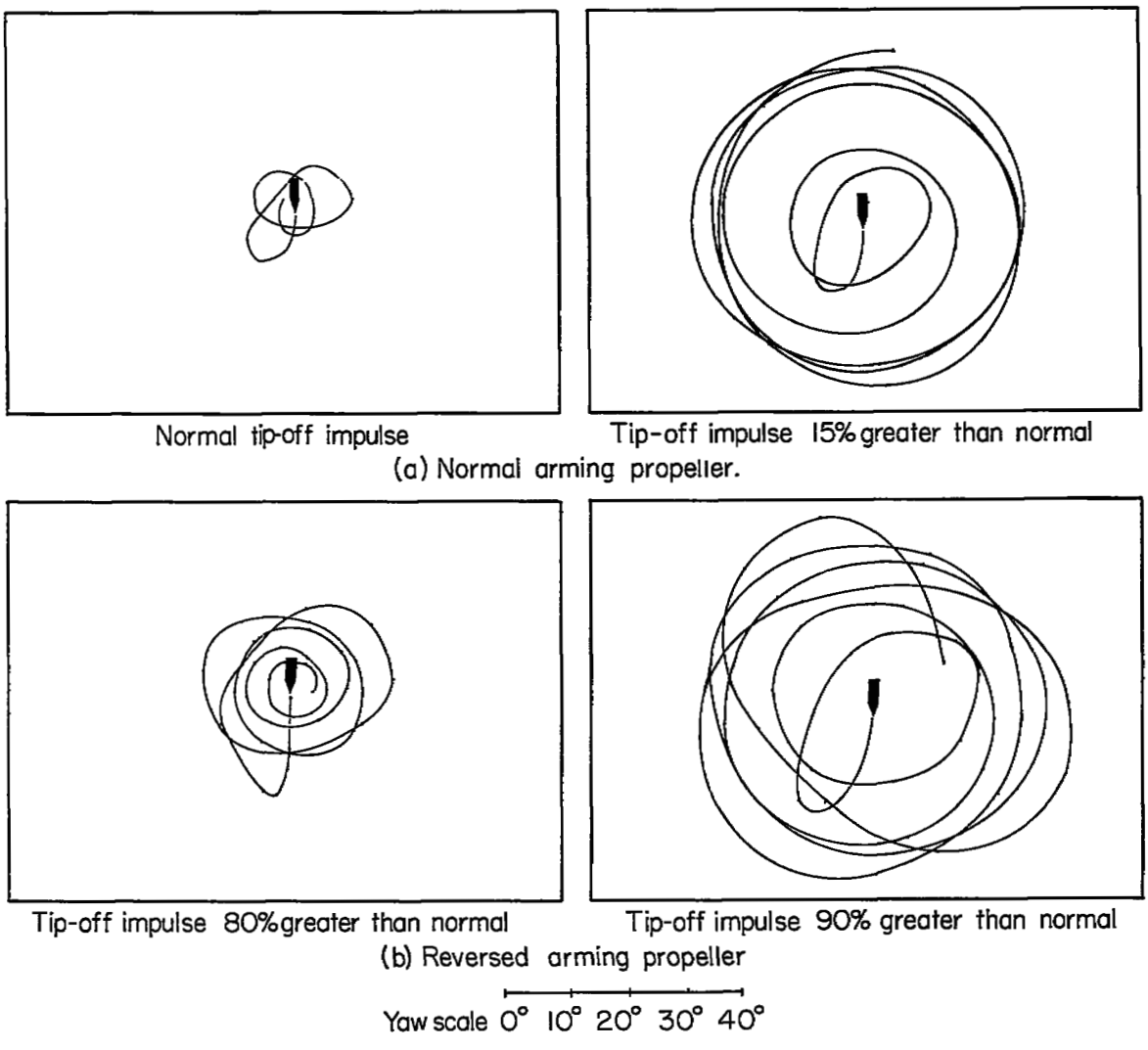

Figure 12.- Calculated motion of the model with the 7° tail and normal spin showing the effect of increasing the magnitude of the tip-off impulse for an initial yaw of 2° tail down, simulating firing directly into the wind. Arrow indicates start of motion and direction of impulse.

[redacted]

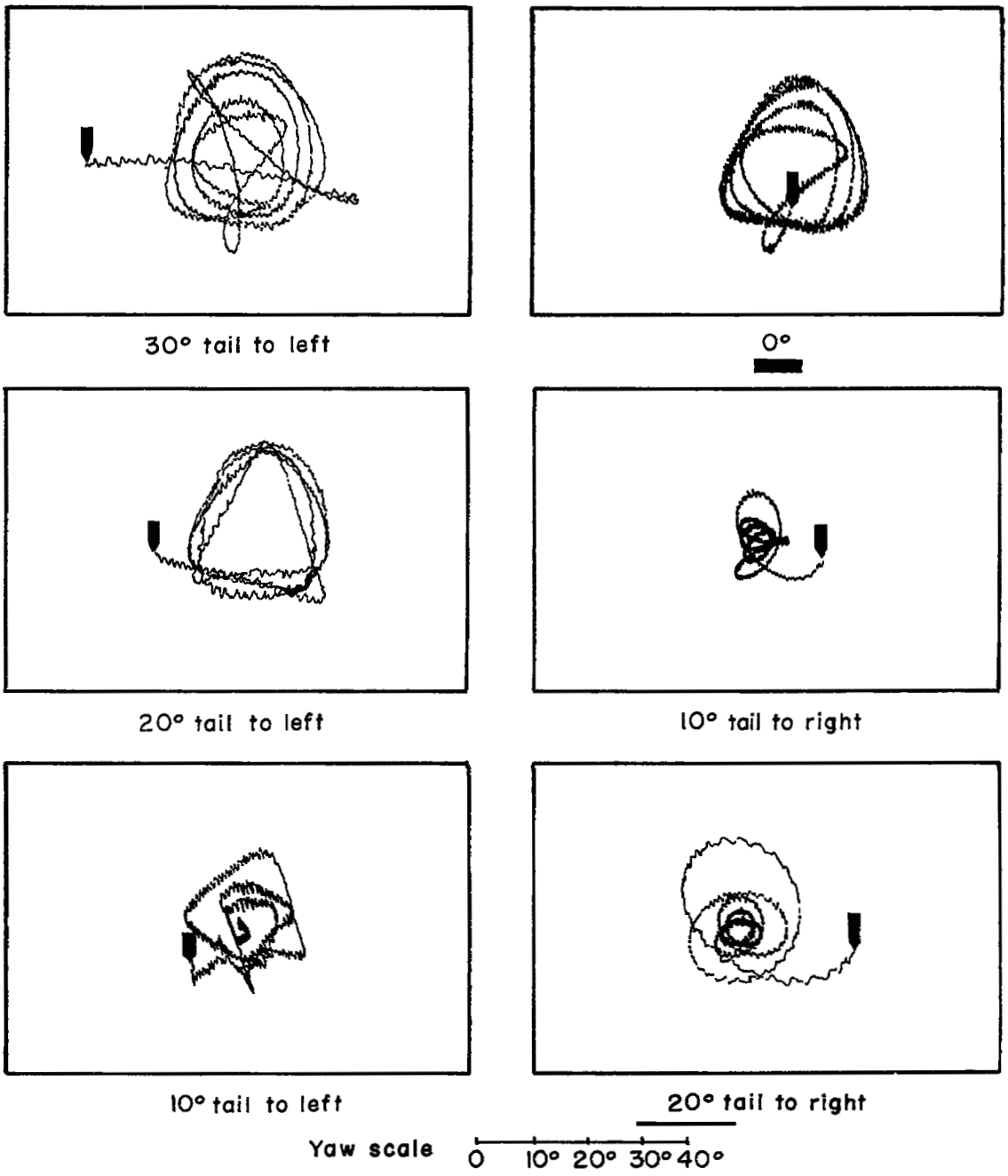

Figure 13.- Experimental motion of model equipped with large reversed-rotation arming propeller and 7° tail for various initial angles of yaw. Tail to left and right simulates firings to port and starboard, respectively. Arrow indicates start of motion and direction of impulse.

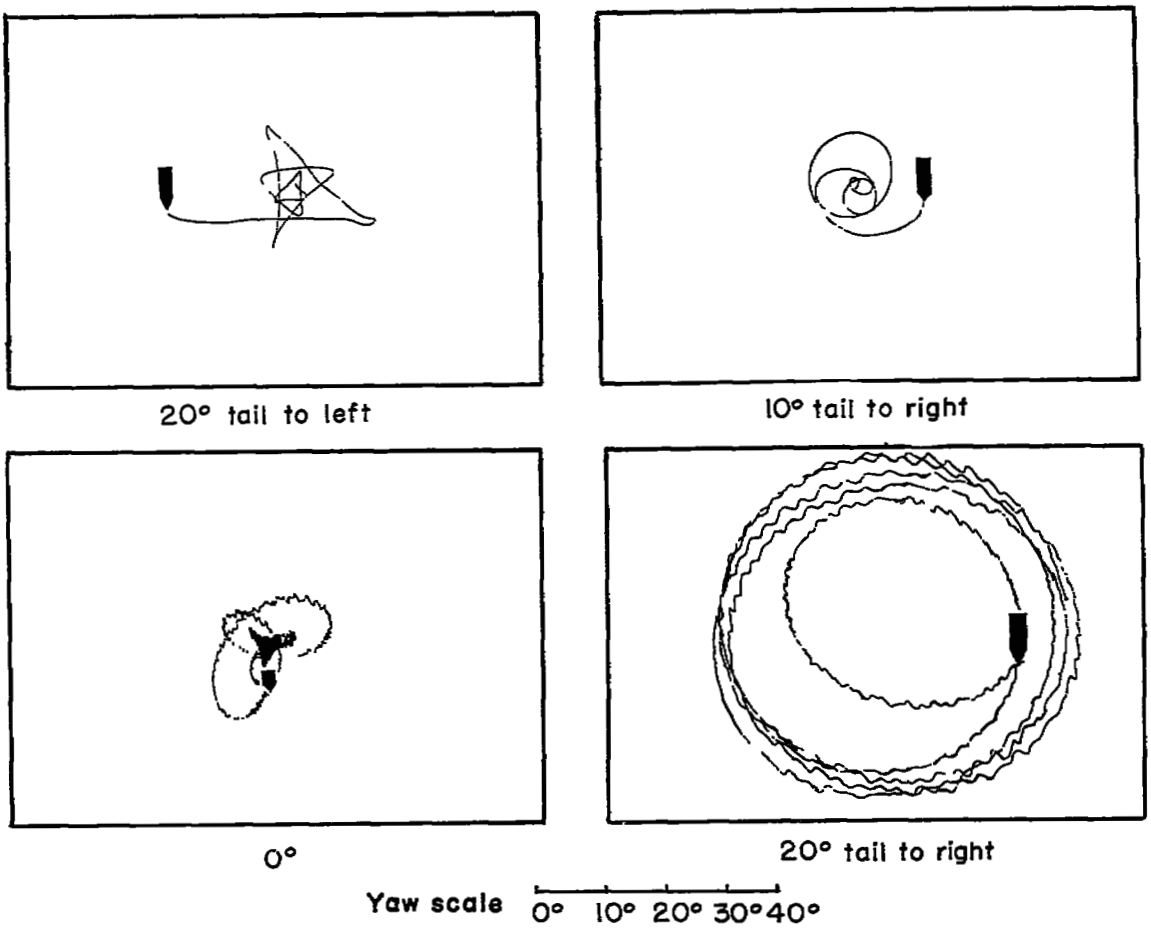

Figure 14.- Experimental motion of model equipped with 7° tail but no arming propeller for various initial angles of yaw. Tail to left and right simulates firings to port and starboard, respectively. Arrow indicates start of motion and direction of impulse.

[redacted]

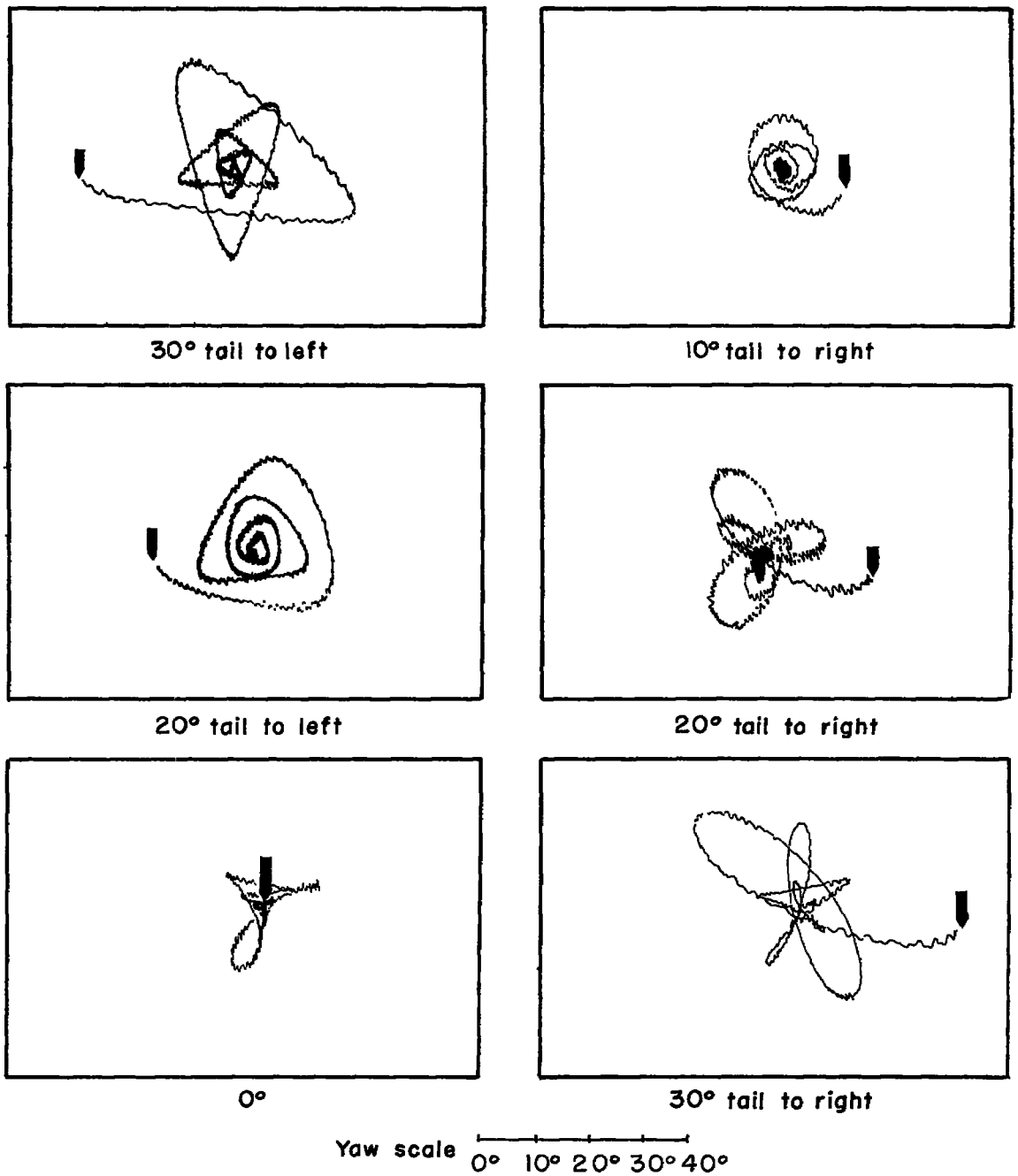

Figure 15.- Experimental motion of model equipped with normal arming propeller, 7° tail, and nose ring for various initial angles of yaw. Tail to left and right simulates firings to port and starboard, respectively. Arrow indicates start of motion and direction of impulse.

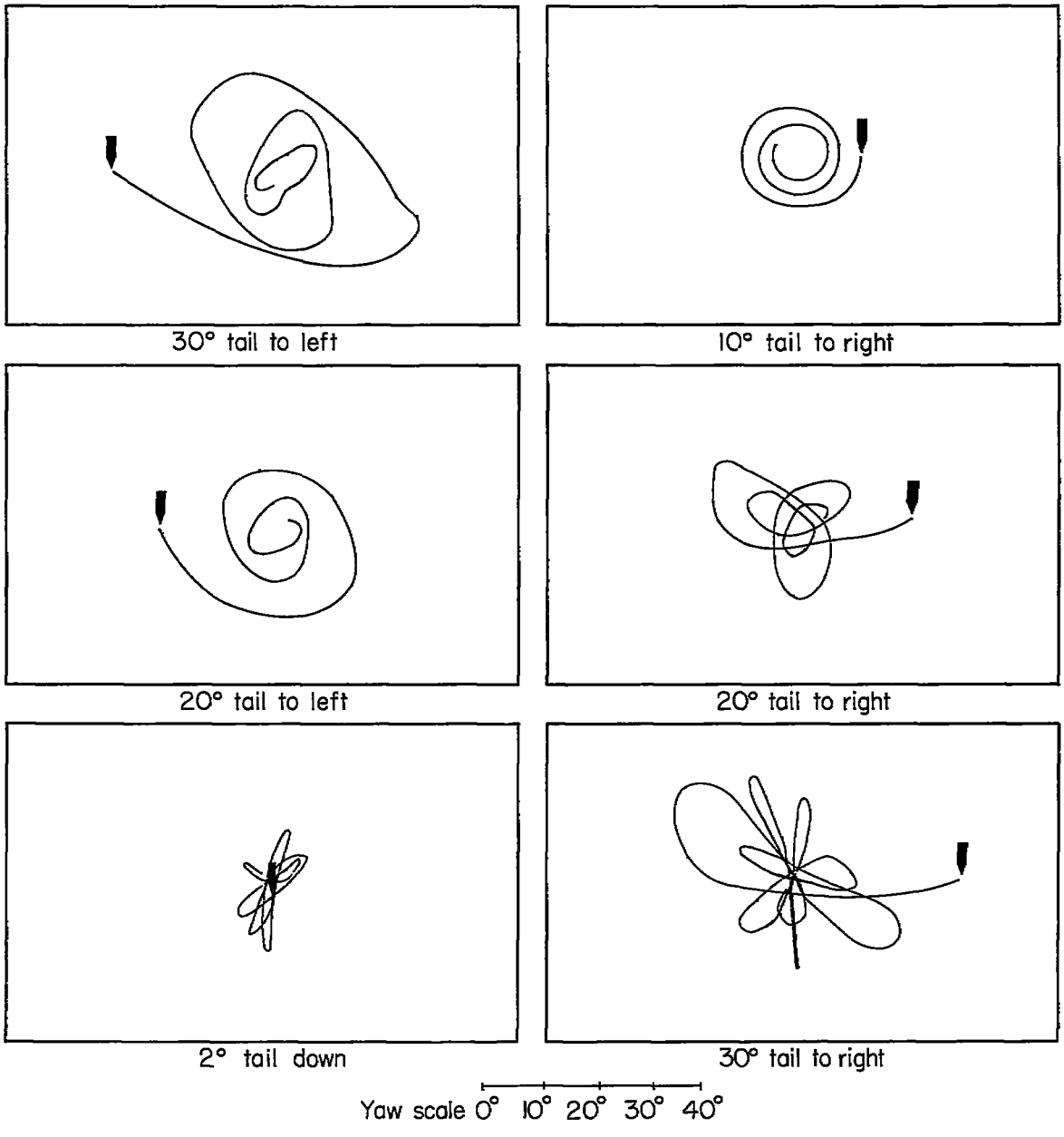

Figure 16.- Calculated motion of model equipped with normal arming propeller, 7° tail, and nose ring for various initial angles of yaw. Tail to left and right simulates firings to port and starboard, respectively. Arrow indicates start of motion and direction of impulse.

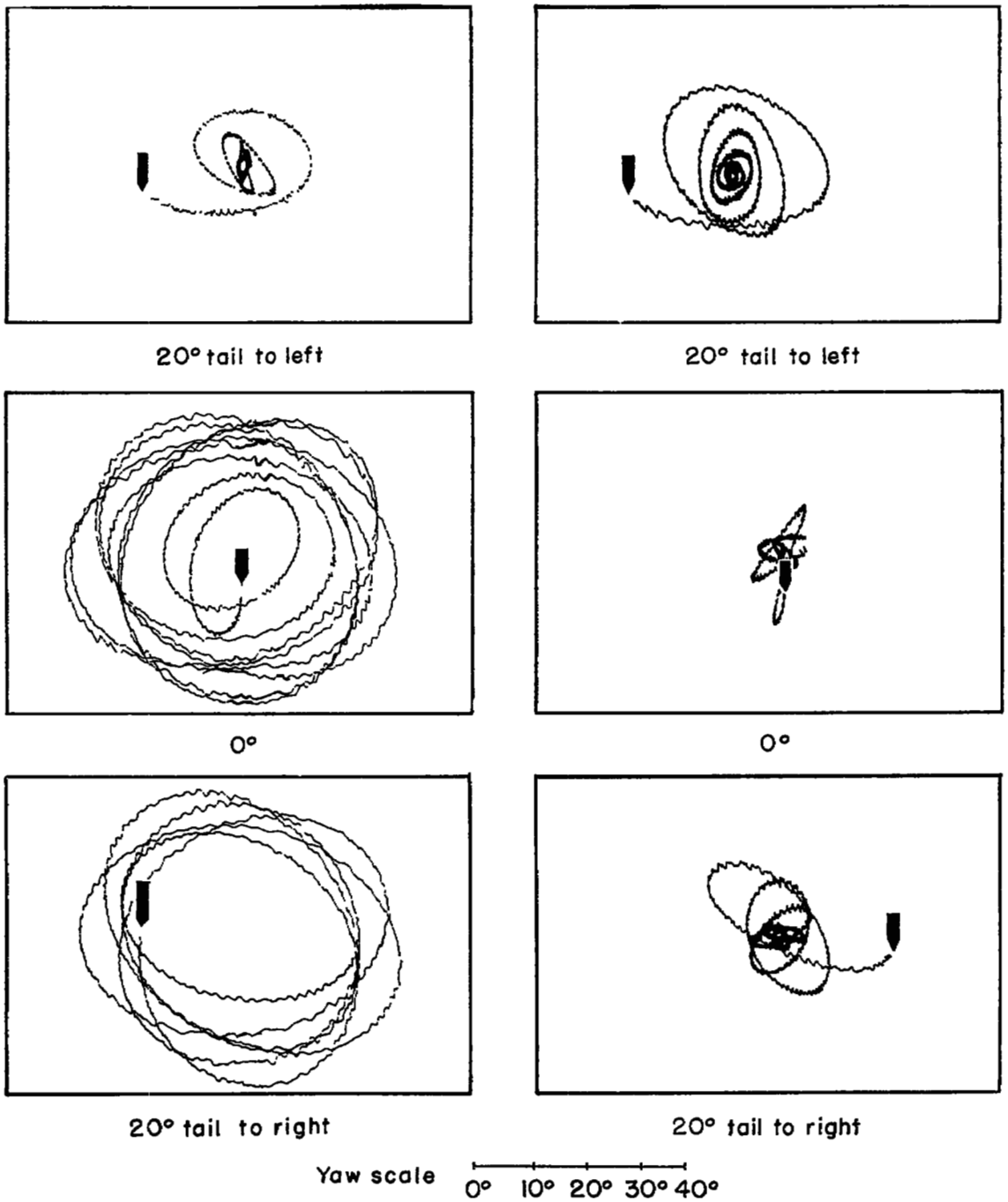

(a) Model without nose ring. (b) Model with nose ring.

Figure 17.- Experimental motion of model equipped with normal arming propeller and 3° tail for various initial angles of yaw. Tail to left and right simulates firings to port and starboard, respectively. Arrow indicates start of motion and direction of impulse.

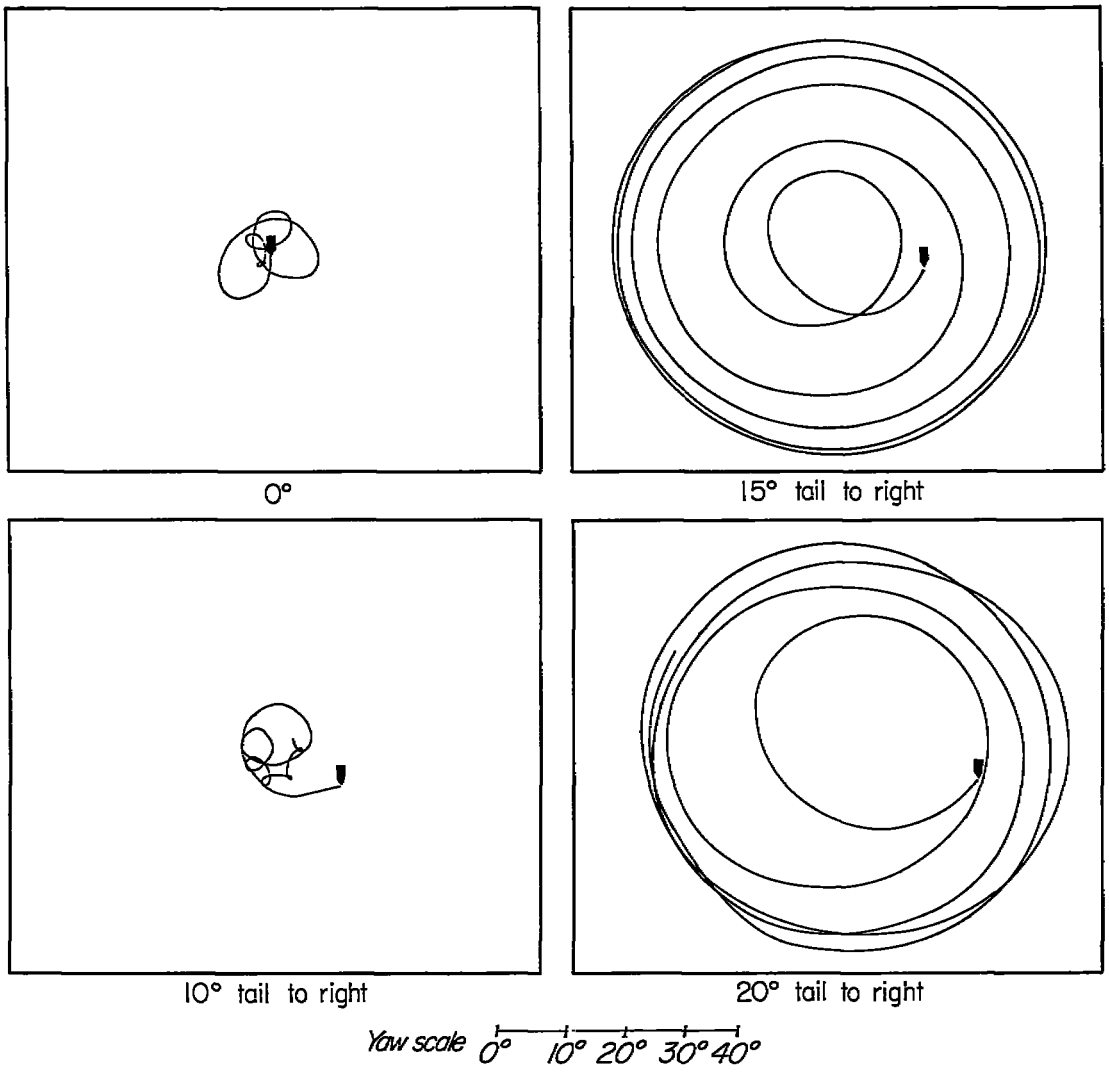

Figure 18.- Experimental motion of model equipped with normal arming propeller and 10° tail for various initial angles of yaw. Tail to right simulates firings to starboard. Arrow indicates start of motion and direction of impulse.

[redacted]

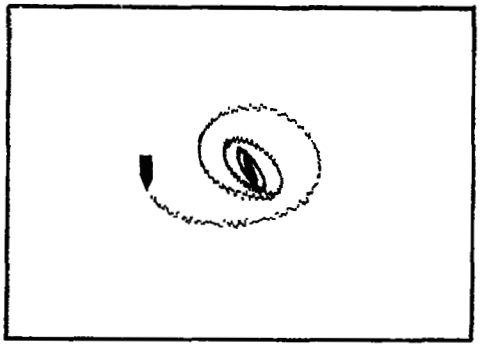

20° tail to left

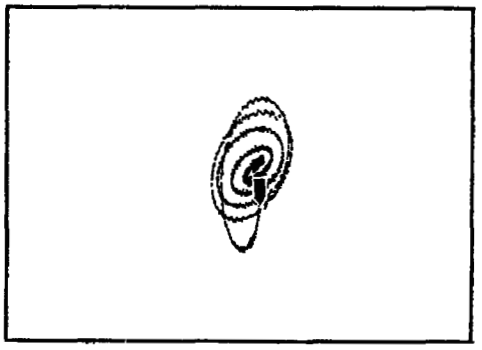

0°

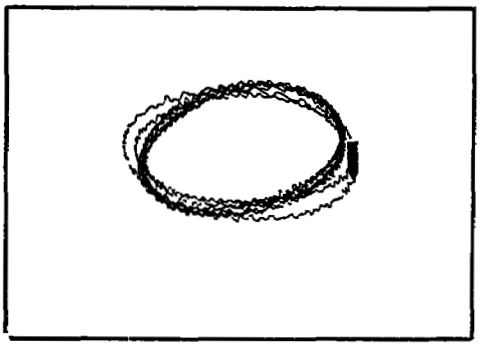

20° tail to right

(a) With normal arming propeller, and without nose ring.

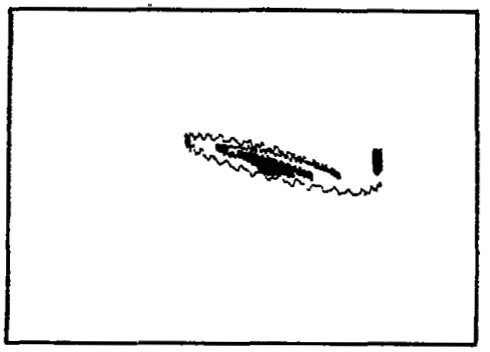

20° tail to right

(b) With normal arming propeller, and with nose ring.

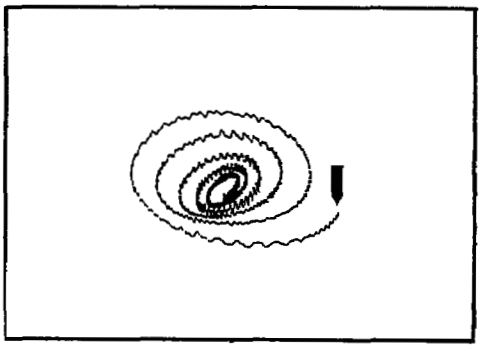

20° tail to right

(c) Without arming propeller and without nose ring.

Yaw scale 0° 10° 20° 30° 40°

Figure 19.- Experimental motion of model equipped with 3° tail but with no spin for various initial angles of yaw. Tail to left and right simulates firings to port and starboard, respectively. Arrow indicates start of motion and direction of impulse.

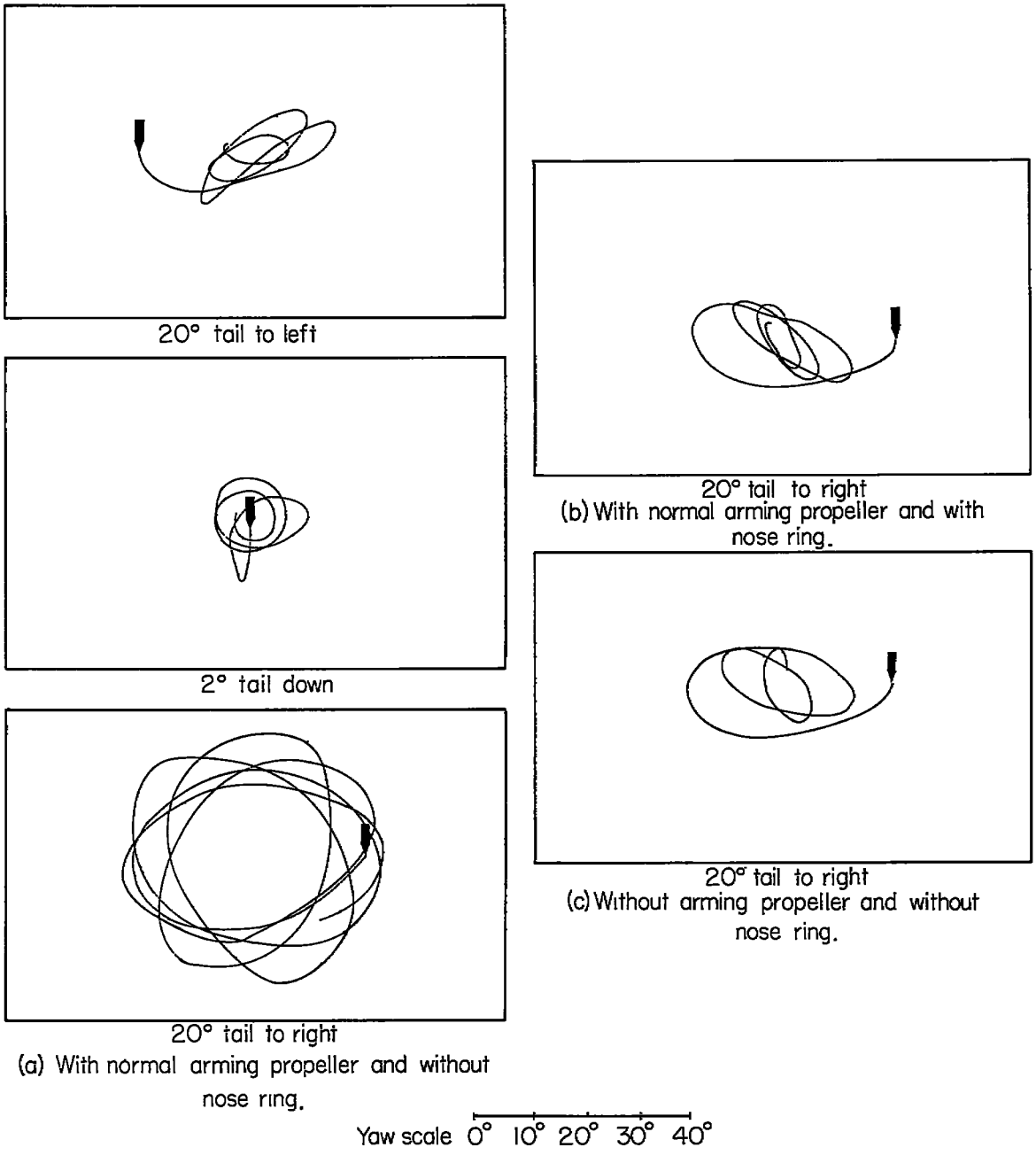

Figure 20.- Calculated motion of model with 7° tail but with no spin for various initial angles of yaw. Tail to left and right simulates firings to port and starboard, respectively. Arrow indicates start of motion and direction of impulse.